doi:10.1093/brain/awn288 *Brain* (2008), **131**, 3311–3334

# Intranasal insulin prevents cognitive decline, cerebral atrophy and white matter changes in murine type I diabetic encephalopathy

George J. Francis,[1] Jose A. Martinez,[1] Wei Q. Liu,[1] Kevin Xu,[1] Amit Ayer,[1] Jared Fine,[2] Ursula I. Tuor,[1] Gordon Glazner,[3] Leah R. Hanson,[2] William H. Frey II[2] and Cory Toth[1]

[1]Department of Clinical Neurosciences and the Hotchkiss Brain Institute, University of Calgary, Calgary, Alberta, Canada, [2]Alzheimer's Research Center at Regions Hospital, HealthPartners Research Foundation, St. Paul, MN, USA and [3]Department of Pharmacology and Therapeutics, Division of Neurodegenerative Disorders, University of Manitoba, St. Boniface Hospital Research Centre, Winnipeg, Manitoba, Canada

Correspondence to: Dr C. Toth, University of Calgary, Department of Clinical Neurosciences, Room 155, 3330 Hospital Drive, N.W., Calgary, Alberta, Canada T2N 4N1
E-mail: corytoth@shaw.ca



**Insulin deficiency in type I diabetes may lead to cognitive impairment, cerebral atrophy and white matter abnormalities. We studied the impact of a novel delivery system using intranasal insulin (I-I) in a mouse model of type I diabetes (streptozotocin-induced) for direct targeting of pathological and cognitive deficits while avoiding potential adverse systemic effects. Daily I-I, subcutaneous insulin (S-I) or placebo in separate cohorts of diabetic and non-diabetic CDI mice were delivered over 8 months of life. Radio-labelled insulin delivery revealed that I-I delivered more rapid and substantial insulin levels within the cerebrum with less systemic insulin detection when compared with S-I. I-I delivery slowed development of cognitive decline within weekly cognitive/behavioural testing, ameliorated monthly magnetic resonance imaging abnormalities, prevented quantitative morphological abnormalities in cerebrum, improved mouse mortality and reversed diabetes-mediated declines in mRNA and protein for phosphoinositide 3-kinase (PI3K)/Akt and for protein levels of the transcription factors cyclic AMP response element binding protein (CREB) and glycogen synthase kinase 3β (GSK-3β) within different cerebral regions. Although the murine diabetic brain was not subject to cellular loss, a diabetes-mediated loss of protein and mRNA for the synaptic elements synaptophysin and choline acetyltransferase was prevented with I-I delivery. As a mechanism of delivery, I-I accesses the brain readily and slows the development of diabetes-induced brain changes as compared to S-I delivery. This therapy and delivery mode, available in humans, may be of clinical utility for the prevention of pathological changes in the diabetic human brain.**

**Keywords:** diabetes; insulin; leukoencephalopathy; white matter abnormalities; brain atrophy; cognitive decline

**Abbreviations:** APP = amyloid precursor protein; CSF = cerebrospinal fluid; DW = diffusion-weighted; EMSA = electrophoretic mobility shift assay; IGF-1 = insulin-like growth factor; IR = insulin receptor; NGF = nerve growth factor; SNMTS = spatial non-matching-to-sample; WMAs = white matter abnormalities

*Received May 27, 2008. Revised October 3, 2008. Accepted October 8, 2008. Advance Access publication November 16, 2008*

## Introduction

Diabetes has been associated with cognitive dysfunction, an elevated risk of dementia, cerebral atrophy and presence of heightened white matter abnormalities (WMAs). Diabetes-associated cognitive dysfunction, first described nearly a century ago (Miles and Root, 1922), occurs in both type of diabetes. In type I diabetes, impaired learning, memory, problem solving skills, and intellectual development have been described (Ryan, 1988; Ryan *et al.*, 1993; Ryan and Williams, 1993; McCarthy *et al.*, 2002; Schoenle *et al.*, 2002). For patients with type I diabetes, the greatest impact of diabetes upon brain structure and function seems to occur at the extremes of age, with little observable effect during the middle adult years (Wessels *et al.*, 2007, 2008; Biessels *et al.*, 2008; Kloppenborg *et al.*, 2008). Also, cognitive dysfunction does not appear to relate to

hypoglycaemic episodes in diabetes (Kramer *et al.*, 1998; Schoenle *et al.*, 2002; Jacobson *et al.*, 2007). Similar cognitive deficits occur in type II diabetic adult patients, with impaired performance on abstract reasoning and complex psychomotor functioning (Reaven *et al.*, 1990; Strachan *et al.*, 1997; Ryan and Geckle, 2000). Diabetes-mediated cognitive changes seem to occur at the two extremes of life: either in childhood (Northam *et al.*, 2001; Schoenle *et al.*, 2002; Fox *et al.*, 2003) or during later stages of life (Stewart and Liolitsa, 1999; Awad *et al.*, 2004; van Harten *et al.*, 2006) when neurodegenerative processes may initiate (Biessels *et al.*, 2008). There are less clear indications that diabetes impacts upon cognitive functioning in middle-age adults (Stewart and Liolitsa, 1999; Awad *et al.*, 2004; Jacobson *et al.*, 2007; Weinger *et al.*, 2008).

In animal models of diabetes, cognitive dysfunction has been demonstrated by impaired performances in the Morris water maze by streptozotocin (STZ)-induced diabetic rats (Biessels *et al.*, 1996, 1998). Both pre- and post-synaptic deficits have been associated with impaired long-term potentiation in the diabetic hippocampus (Biessels *et al.*, 1996; Kamal *et al.*, 2006). Short-term replacement of insulin in STZ-treated rats from the onset of diabetes prevents cognitive decline and protects against hippocampal potentiation deficits, but cannot reverse these electrophysiological changes (Biessels *et al.*, 1998). Long-term protection against development of diabetic encephalopathy via locally delivered insulin has not yet been attempted.

Structural defects within the diabetes-exposed brain include cerebral atrophy identified with neuroimaging techniques (Schmidt *et al.*, 2004; Manschot *et al.*, 2006; Musen *et al.*, 2006; Ikram *et al.*, 2008; Last *et al.*, 2007). Cerebral atrophy, possibly acting in concert with WMA, is associated with cognitive decline (Whitman *et al.*, 2001; Manschot *et al.*, 2006). Diabetes is a risk factor for WMA presence in some studies (Pantoni and Garcia, 1997; Murray *et al.*, 2005; Akisaki *et al.*, 2006; Manschot *et al.*, 2006; Musen *et al.*, 2006; van Harten *et al.*, 2007), but not in others (Schmidt *et al.*, 2004). By themselves, WMAs in humans are a risk factor for stroke (Knopman *et al.*, 2001), cognitive deficits (Pantoni *et al.*, 2007) and abnormalities in gait associated with falling (Schwartz *et al.*, 2008). The presence of cerebral atrophy or WMA has been linked to cognitive dysfunction in a number of human studies (Manschot *et al.*, 2006; Verdelho *et al.*, 2007). Rodent models of diabetes have also demonstrated cerebral atrophy (Lupien *et al.*, 2006; Toth *et al.*, 2006) and WMAs (Toth *et al.*, 2006) due to long-term diabetes. Such pathological changes have been associated with cognitive decline over time in mouse models of diabetes (Toth *et al.*, 2006) and in diabetic rats where hippocampal electrophysiological changes were present (Biessels *et al.*, 1996; Kamal *et al.*, 2000). One pathogenic factor related to presence of brain atrophy and WMA in experimental diabetes is the presence of the receptor for advanced glycation end products (RAGE) (Toth *et al.*, 2006). However, another important factor may be relative impaired insulin levels and activity in the brain exposed to diabetes (Li *et al.*, 2005; Haan, 2006), as described in the human Alzheimer's disease brain (Craft *et al.*, 1998; Hoyer, 2004). Insulin receptors (IRs) are present at central neurons, synapses, and upon glia (Adamo *et al.*, 1989; Unger *et al.*, 1989; Wickelgren, 1998; Abbott *et al.*, 1999; Zhao *et al.*, 2004*a*); therefore, it is assumed that insulin and its signalling play an important role in neuronal, glial, and overall cognitive and memory functioning. Insulin replacement within the central nervous system may prevent or even reverse such diabetes-associated changes, although its systemic delivery is complicated by hypoglycaemia. Also, potentially impaired function of the blood–brain barrier may prevent insulin transport from achieving sufficient cerebral levels (Cohen, 1993; Mooradian, 1997; Hattori *et al.*, 2000; Kaiyala *et al.*, 2000). An alternative method of delivering insulin to the brain could be instrumental in preventing diabetes-accelerated neurodegeneration.

Intranasal administration permits insulin or similar peptides to bypass the periphery and the blood–brain barrier (Dhanda *et al.*, 2005), reaching the brain and entering the cerebrospinal fluid (CSF) within minutes. Proteins with size of up to 20 kDa, including insulin, insulin-like growth factor (IGF)-1 and nerve growth factor (NGF), have been successfully delivered to the brain using this method (Chen *et al.*, 1998; Liu *et al.*, 2004; Ross *et al.*, 2004; Thorne *et al.*, 2004; Reger *et al.*, 2006, 2008; Vig *et al.*, 2006). Transport of molecules delivered intranasally occurs through extracellular bulk flow transport along olfactory and trigeminal perivascular channels, as well as possibly through axonal transport pathways (Benedict *et al.*, 2004; Thorne *et al.*, 2004; Reger *et al.*, 2006). This technique permits targeted delivery to the brain to assess the direct effect of insulin upon its receptors without significant changes in plasma insulin or glycaemic levels (Patti *et al.*, 1995; White and Yenush, 1998; Leinninger *et al.*, 2004; Reger *et al.*, 2006, 2008; Yu *et al.*, 2006).

We hypothesized that long-term replacement of insulin within the experimental type I diabetic mouse brain could slow or prevent such changes. Insulin's ligation to highly expressed IR in brain regions including the hippocampus and upon synapses (Abbott *et al.*, 1999), may promote learning and memory (Zhao *et al.*, 2004*a*). We used daily intranasal delivery of insulin over a life span while performing behavioural and neuroimaging measures to monitor progression. These studies were also performed to assist in delineation of insulin's trophic and anti-hyperglycaemic effects upon development of diabetic encephalopathy. Given the absence of neuronal loss in prior studies of the diabetic murine brain (Toth *et al.*, 2006), we also examined for evidence of synaptic loss, as well as the previously detected myelin loss. We postulated that intranasal insulin delivery would sustain the diabetic nervous system, potentially limiting cognitive decline, brain

atrophy and WMAs, while limiting serious systemic side-effects that could occur with systemic insulin delivery.

## Materials and Methods

### Animals

We studied a total of 484 male Swiss Webster wild-type (wt) mice with initial weight of 20–30 g, in strict pathogen-free plastic sawdust-covered cages with a normal light–dark cycle and free access to mouse chow and water. All protocols were reviewed and approved by the University of Calgary Animal Care Committee using the Canadian Council of Animal Care guidelines. Mice were anaesthetized with pentobarbital (60 mg/kg) prior to all procedures. At the age of 1 month, 304 mice were injected with streptozotocin (Sigma, St. Louis, MO) intraperitoneally with once daily doses with each of 60 mg/kg, 50 mg/kg and then 40 mg/kg over three consecutive days, while the remaining 180 mice were injected with volume-equated placebo carrier (sodium citrate) for 3 consecutive days. One hundred and forty-four mice injected with STZ and 80 mice injected with carrier were held aside for morphological studies to be performed at 1, 3 and 5 months after injections; the remaining mice were followed for the entire length of the study (8 months of diabetes or equivalent for carrier-injected mice) as mortality permitted. Monthly weights were obtained and monthly whole-blood glucose measurements were performed using the tail vein and a blood glucometer, (OneTouch Ultra Meter, LifeScan Canada, Burnaby, BC, Canada) with hyperglycaemia verified 1 week after STZ injection; a fasting whole-blood glucose level of $\geqslant$16 mmol/l (normal 5–8 mmol/l) was our criterion for experimental diabetes. In all cases, those mice that did not develop diabetes as defined above following STZ injections were excluded from further assessment. Animals were inspected twice daily, and examined for signs of depressed level of consciousness, ataxia or general malaise. When such signs were identified, whole-blood glucose testing was performed, with a measurement of $<$3.5 mmol/l defined to represent hypoglycaemia. No intervention was performed at any time with regards to additional insulin, glucose or fluid delivery. In situations where the mouse was obviously ill, euthanasia was performed. In circumstances where severe hyperglycaemia was found (>33 mmol/l) in an ill mouse, euthanasia was again performed.

We studied cohorts with a maximum of eight mice in each group initially due to resource limitations. After the initial cohorts containing eight mice each were studied, a second cohort was used to obtain additional mouse data for mouse cohorts with higher levels of mortality. For any animal that experienced mortality after the 20-week point of the cognitive studies, their data were carried through using the last obtainable data point.

### Intranasal insulin or saline delivery

$^{125}$I-labelled I-I and subcutaneous insulin (S-I) administration were performed at the University of Minnesota for determination of targeting of insulin delivery methods. This procedure was approved by the institutional animal care and use committee at Regions Hospital. Prior to experimentation, 21 non-diabetic animals were acclimated to handling for awake intranasal delivery over ~2 weeks. $^{125}$I-labelled I-I was provided to 12 Swiss Webster mice (male, 6–8 weeks, Charles River) and $^{125}$I-labelled subcutaneous insulin S-I was provided to nine mice under pentobarbital anaesthesia (60 mg/kg). Insulin (Humulin R, Eli Lilly, Toronto, Canada) with an initial concentration of 100 U/ml or 4033.98 mg/ml was dissolved in PBS and custom-labelled with $^{125}$I (GE Healthcare, Piscataway, NJ, USA). Synthesized radiolabelled insulin solution contained 344.3 μCi/ug. $^{125}$I-labelled I-I delivery was performed in a fume hood behind a lead-impregnated shield, with anaesthetized mice placed supine. A mixture of $^{125}$I insulin (15.8 μCr) and unlabeled insulin (3.3 μg) were administered as I-I or S-I. $^{125}$I I-I was delivered over alternating nares as eight 3-μl drops with an Eppendorf pipetter every 2 min, for a total volume of 24 μl. This schedule of delivery has been modified from a previously used method in rats to quantify radiolabelled delivery of molecules within the Frey laboratory (Thorne *et al.*, 2004). For subcutaneous delivery, $^{125}$I S-I was delivered with a single subcutaneous injection of 24 μl in a fume hood behind a lead-impregnated shield. Each desired dose contained a calculated radioactive dose of 30 μCi.

At each of 1, 2 and 6 h after initiating $^{125}$I I-I or S-I delivery, cardiocentesis was performed for blood extraction, followed by performance of euthanasia via transcardial perfusion using 120 ml of 4% paraformaldehyde while the mouse was maintained under anaesthesia. To quantify $^{125}$I distribution, blood, urine, lymphatic and visceral organ structures, as well as portions of the central and peripheral nervous systems were harvested. Gamma signal was recorded for each body region with autoradiographic imaging using a phosphor screen. Concentrations of $^{125}$I insulin were calculated based upon the gamma counting data, tissue weight, specific activity of the insulin administered and standards measured. Results were studied for penetration into peripheral nervous system tissues (reported elsewhere) and central nervous system tissues.

Daily I-I (Humulin R, Eli Lilly, Toronto, ON) or intranasal saline (I-S) was administered to both diabetic and non-diabetic male Swiss Webster mice over 8 months of diabetes. A total of 24 μl containing either a total of 0.87 U of insulin or 0.9% saline only was provided as four 6-μl drops by an Eppendorf pipetter over alternating nares every minute while each mouse was held in supine position with neck in extension. Daily S-I (0.87 U/d, Humulin R, Eli Lilly, Toronto, ON) and subcutaneous saline (S-S) were also administered to either diabetic or non-diabetic male Swiss Webster mice. All therapies began immediately after confirmation of presence of diabetes for each cohort. In the first week, daily glucometer testing was performed for all mice, followed by once-a-month testing. In this work, mice with diabetes were indicated with a 'D', while mice without diabetes (control mice) are indicated with a 'C'. Delivery of subcutaneous saline is indicated as 'S-S', subcutaneous insulin as 'S-I', intranasal saline as 'I-S' and intranasal insulin as 'I-I'.

We attempted to use other control groups, but their utility was limited in each case. First, we attempted to use subcutaneous insulin via a sliding scale approach in six diabetic mice in order to maintain normal or mildly high glycaemia levels. This approach required daily checks of whole-blood glucose using a tail vein; over the span of 1 month, all of the six diabetic mice developed infection over the tail, leading to amputation in three mice (50%) and was probable cause of death in two mice (33%). During the course of an 8-month-long study, the morbidity associated with this procedure would be unacceptable and confounding. We also attempted to maintain a protected venous catheter in the tail vein for obtaining whole-blood glucose, but this was associated with auto-removal of the catheter and failure at re-insertions due to fibrosis of tail tissues. We also studied six diabetic mice receiving

a half dose of the desired I-I dose (0.43 U/d) over 1 month. One mouse (17%) died of confirmed hypoglycaemia, with the other five mice surprisingly had no statistical difference in glycaemic levels when compared to a complementary group of six diabetic mice receiving subcutaneous placebo injections. Therefore, we selected the S-I dose to be equivalent to the I-I dose for the cohorts studied.

## Behavioural testing

A minimum of eight mice in each cohort [32 diabetic (D I-I, D I-S, D S-I and D S-S) and 32 control mice (C I-I, C I-S, C S-I and C S-S)] had cognitive behavioural testing performed once weekly for evaluation of procedural, visuospatial and recognition memory. All behavioural tests were conducted under regular light between 09:00 and 15:00 h after fasting overnight from 19:00 onwards. Every mouse was trained in each test paradigm for 3 weeks before initiation of test recording and prior to diabetes initiation, beginning after 2 weeks of diabetes at 1.5 months of age. Behavioural equipment was maintained in the identical position and climate on each occasion and was recorded by the same observers in order to ensure stability of distant navigational cues provided by objects around the testing. Testing always occurred in the order of Holeboard test, Radial arm test, Object Recognition test (each performed while fasting) followed by feeding and then the Morris Water-Maze test 1 h later. While the Holeboard and Radial Arm tests evaluate spatial information processing and memory, the Morris Water Maze also evaluates procedural memory and aversive motivation. In contrast, the Object Recognition test evaluates novelty seeking and exploratory behaviour. Each mouse performed one trial of each test per week. Due to the possibility of motor limitations confounding the results of cognitive testing, concurrent testing of linear swim speed and linear running speed were performed monthly; once measurable differences in motor function occurred between interventional groups in swim or run speed, cognitive testing was discontinued.

The Radial Arm test maze consists of a central platform (35 cm in diameter) and eight arms (each 76 cm long and 12 cm wide) constructed of black plastic projecting radially from the platform with adjacent arms separated by 45° (Schwabe *et al.*, 2006). A food reward (Cheerio) is placed in the same arm each occasion at 180° from the starting point of the mouse placed in the middle of the central platform. A mouse was recorded as entering an arm when it passed the midpoint of the arm in a centrifugal fashion. Each trial ended when the reward was collected or when 720 s expired. Variables recorded during each test were latency for collecting reward and the number of errors made, defined as a re-entry into an arm previously entered, classified as a reference memory error.

The Holeboard test was modified from a previous reported design (File and Wardill, 1975), and was composed of a rectangular open field (60 × 90 cm) made of opaque white acrylic surrounded by opaque walls 60 cm high. Eight holes (2.5 cm diameter) were placed in two lines of four, equidistant from each other and from the walls. Each mouse was started in the same corner while the food reward (Cheerio) was placed in the same hole (second hole in the far row, kitty-corner from the starting point). The latency to collect the reward and the number of times the mouse placed its head in each individual hole was recorded, with errors defined as repeat visit of a previously visited hole, classified as a reference memory error.

The Object Recognition task was performed in an open wooden box (60 × 60 × 60 cm) with unique objects to be discriminated constructed from children's blocks. On the day of the test, at the first 2-min sample trial (T1), two identical objects (termed as sample objects) were presented in two corners of the box. Then, in the second 2-min choice trial (T2) performed 30 min later, one of the objects presented in T1 was replaced by a new object. Objects were cleaned between trials and between mouse to prevent the possibility of scent traces forming an olfactory cue. The time (in seconds) as well as the number of visits taken by mice in exploring objects in the two trials were recorded, with exploration considered as directing the nose to the object at a distance $\leqslant$2 m and/or touching it with the nose. This paradigm has been termed delayed 'spatial non-matching-to-sample' (SNMTS) testing (Rothblat and Kromer, 1991).

A mouse-adapted Morris water-maze task (Morris, 1984; Crawley, 2000; Whishaw and Kolb, 2005) was performed after feeding and used a solid-coloured circular pool 88 cm in diameter and 20 cm in height filled with water at 25°C. The position of the 10 cm radius hidden platform remained fixed for all testing over the entire study period, and each mouse was placed at an identical starting position opposite the hidden platform. Animals were left to swim until either they located the platform, climbing upon it and staying for at least 2 s, or when 300 s elapsed. Post-testing, mice were placed under a heating lamp to warm. Variables recorded during each test were latency to reach the platform (escape latency) and the fraction of time spent within the hemisphere of the pool containing the platform (thigmotaxis).

## Magnetic resonance imaging

At each month of diabetes, four mice from each cohort [16 diabetic (D I-I, D I-S, D S-I and D S-S) and 16 control mice (C I-I, C I-S, C S-I and C S-S)] underwent magnetic resonance (MR) scanning at the Experimental Imaging Centre at the University of Calgary. MR images were obtained in animals anaesthetized by mask with isoflurane using a quadrature volume coil and a Bruker 9.4 Tesla MR imaging system. Respiration and temperature were monitored and inner core temperature was maintained to be within 36–37°C with a heated air feedback system. The head was restrained using ear pins. Three different sets of MR scans were performed using sequences that acquired $T_1$-weighted images, diffusion-weighted (DW) images for calculating an apparent diffusion coefficient of water (ADC) map and $T_2$-weighted images for determining $T_2$ maps within a total of 24 slices through the cerebrum. $T_1$-weighted images were acquired using a spin echo sequence with a repetition time (TR) of 500 ms and an echo time (TE) of 8 ms. Diffusion-weighted (DW) images were acquired using a spin echo sequence with TR/TE = 1200/49 ms and b values of 46 and 767 s/mm$^2$, respectively. $T_2$ maps were obtained from multi-spin-echo images at TR = 1200 ms, 12 echoes and TE = 12.5 ms. The field of view was 2 × 2 cm, with an acquisition matrix of 256 × 256 and a slice thickness of 0.75 mm. MR images of brain were analysed using locally available software (Marevisi, IBD) by an observer blinded to the treatment group. Calculation of $T_2$ values, perfusion values, and ADC values within brain regions of interest were performed bilaterally for each of the control and diabetic animals. Apparent visualized abnormalities in $T_1$- and $T_2$-weighted images were also recorded for each animal. In addition, MR images were used to calculate brain widths at pre-determined anatomical landmarks as well as to measure

overall brain volume. Volumetric brain measurements were calculated as a summation of cross-sectional areas for each slice multiplied by the thickness of the MR slices.

## Tissue harvesting

Prior to sacrifice after 1, 3, 5, 7 or 9 months of diabetes, animal weights and blood glucoses were determined. A total of 0.5 ml of whole intracardiac blood was obtained for glycated haemoglobin measurements to be performed with affinity chromatography (Procedure 422; Sigma Diagnostics). Euthanasia for animals was performed with an overdose of pentobarbital intraperitoneally, followed by harvesting of brain tissues, placement of half of all brain tissues in 2% formaldehyde and embedding in paraffin. For these specimens, 10 µm sections were cut for morphological and immunohistochemical studies. The other half of mouse brain tissues were placed in Trizol reagent (Life Technologies Inc., Rockville MD, USA) or liquid nitrogen for quantitative real-time reverse transcriptase polymerase chain reaction (qRT-PCR) and Western blot studies respectively with storage at –80°C for a maximum of 1 month.

## Brain sectioning and staining

Degrees of myelination were determined by staining paraffin brain sections for either Luxol Fast Blue (LFB) or myelin basic protein (MBP) (1:100, Stemcell Technologies Inc., Vancouver). For LFB staining, slides were de-waxed and stained in LFB overnight at 37°C followed by alcohol washing and subsequent differentiation of the stain with 0.05% lithium carbonate and then alcohol. Slides used for MBP detection were incubated in methanol for 20 min and washed in phosphate-buffered solution (PBS), then incubated in Triton-X for 30 min before blocking with 10% normal bovine serum for 1 h. Following PBS washes, slides were incubated with mouse anti-MBP overnight followed by incubation with the secondary antibody (bovine anti-mouse IgG Cy3, 1:100 Zymed Inc., San Francisco) for 1 h.

Brain sections stained for LFB were chosen to reflect pre-defined regions of interest (Appendix 1), representing those regions known to be abnormal within diabetic human brains, as well as cortical and subcortical regions important in memory and cognition (Munoz *et al.*, 1993; de Groot *et al.*, 2000; Tullberg *et al.*, 2004; Toth *et al.*, 2006). Assessment of MBP labelling was performed using Image Pro Plus software (Image Pro Plus 5.0, MediaCybernetics, Silver Spring, MD) in order to measure the optical density or degree of immunofluorescence within each brain region of interest. LFB staining was assessed using optical density measurements with Photoshop software for quantification of blue. All assessments of brain sections were performed by an investigator blinded to the experimental conditions.

Additional immunohistochemistry was performed to identify neurons with microtubule-associated protein (MAP)-2, and to identify oligodendrocytes with PDGFRα immunohistochemistry. Background staining was blocked using 1% bovine serum albumin for 1 h, and then slides were stained with monoclonal mouse anti-MAP-2 (1:100, Abcam, Cambridge, MA) or PDGFRα (1:100, Abcam, Cambridge, MA) for neuron and oligodendrocyte detection, respectively. The secondary antibody used was anti-mouse IgG Cy3 (1:100, Zymed Inc., San Francisco) in both cases.

Detailed counts of both neuronal and oligodendroglial cell numbers within grey matter areas of interest (Appendix 1) were performed using standard unbiased stereological methods for those slides stained with the neural marker MAP-2 (Gundersen *et al.*, 1988; Toth *et al.*, 2006) and the oligodendroglial marker PDGFRα. Volume and total cell number were performed with the examiner blinded to the condition and treatment of each mouse brain. Twelve sampled areas were counted for each brain region in each brain, with neurons distinguished based upon nuclear size and appearance.

## Quantitative real-time PCR

Total RNA was extracted from brain regions stored in Trizol reagent (Life Technologies Inc., Rockville, MD). Total RNA (1 µg) was processed directly to cDNA synthesis using the TaqMan\Reverse Transcription Reagents kit (Applied Biosystems). All PCR primers and TaqMan probes were designed using software PrimerExpress (Applied Biosystem) and published sequence data from the NCBI database. PI3K primer sequences were: forward, 5′-AACCCGGCACTGTGCATAAA-3′; reverse 5′-GCCCATT GGATTAGCATTGATG-3′. Akt primer sequences were: forward, 5′-TCTGCCCTGGACTACTTGCACT-3′, reverse, 5′-GCCCGAAGT CCGTTATCTTGA-3′. NFkBp65 primer sequences were: forward, 5′-TGTGCGACAAGGTGCAGAAA-3′; and reverse, 5′-ACAATG GCCACTTGCCGAT-3′. β-actin primer sequences were: forward, 5′-TGTTGTCCCTGTATGCCTCTGGTC-3′; reverse, 5′-ATGTCA CGCACGATTTCCCTCTCTC-3′. SYP primer sequences were: forward, 5′-AAAGGCCTGTCCGATGTGAAG-3′; reverse, 5′-TCCC TCAGTTCCTTGCATGTG -3′. ChAT primer sequences were: forward, 5′-CTATGAGAGTGCATCCATCCGC-3′; reverse, 5′-GG TCAGTCATGGCTTGCACAA-3′.

RT-PCR was performed using SYBR Green dye. All reactions were performed in triplicate in an ABI PRISM 7000 Sequence Detection System. Data were calculated by the $2^{-\Delta\Delta CT}$ method and are presented as the fold induction of mRNA for RAGE in diabetic tissues normalized to $^{18}S$ for comparison to non-diabetic tissues (defined as 1.0-fold).

## Western blot

Thalami and sensorimotor cortices from brains for each cohort were homogenized using a RotorStator Homogenizer in ice-cold lysis buffer (10% glycerol, 2% SDS, 25 mM Tris–HCl, pH 7.4, Roche Mini-Complete Protease Inhibitors). Samples were then centrifuged at 10 000 *g* for 15 min. Supernatant was stored at –20°C prior to SDS–PAGE and immunoblotting analysis. Equal amounts (150 µg) of protein were loaded and samples were separated by SDS–PAGE using 10% polyacrylamide gels with 800 V-h of current applied. Separated proteins were transferred onto nitrocellulose paper (BioRad) over 16 h at 200 mA in Towbin transfer buffer (25 mM Tris, 192 mM glycine, 20% v/v methanol, 0.1% v/v SDS). The blot was blocked for 1 h in 7.5% (w/v) milk (Nestle, Carnation) in TBS [50 mM Tris, 137 mM NaCl, 51 mM KCL, 0.05% (v/v) Tween-20]. The PI3K and Akt pathway were investigated with PI3K (1:1000), PKB/Akt (1:1000), pAkt (1:1000). The nuclear signalling transcription factor NFkB p65 and p50 subunits (1:1000 each) were also examined, and additional immunohistochemistry was performed for CREB (1:200, Abcam Inc., Cambridge, MA) and glycogen synthase kinase 3β (GSK3β) (1:200, Abcam Inc., Cambridge, MA). Quantification of synaptic presence was performed using anti-synaptophysin (SYP) (1:1000; Santa Cruz, Santa Cruz, CA, USA, polyclonal) and Anti-Choline Acetyltransferase (ChAT) (1:500, Abcam, Cambridge,

UK, polyclonal). Identification of proteins for IRβ (C-19) (1:500, Santa Cruz Biotechnology Inc., Santa Cruz, CA, USA) and insulin (1:500, Abcam, Cambridge, UK, polyclonal) were also performed using Western blotting. For a housekeeping protein, anti-β-actin (1:100, Biogenesis Ltd. Poole, UK) was applied to separate blots. Secondary anti-rabbit, anti-mouse or anti-human IgG HRP Linked antibody (Cell Signaling) was applied at 1:5000 in each case as appropriate. Signal detection was performed by exposing of the blot to enhanced chemi-luminescent reagents ECL (Amersham) for 2 min. The blots were subsequently exposed and captured on Kodak X-OMAT K film. In each case, three blots were performed, and analysed with Adobe Photoshop (Adobe Photoshop 9.0, Adobe, San Jose, CA, 2005) for quantification of relative protein content.

Analysis of Western blots used a ratio of protein of interest to β-actin protein for each region of brain tissue and each cohort. Quantification of the luminosity of each identified protein band was performed using Adobe Photoshop software (Adobe Photoshop 7.0, Adobe, San Jose, CA, 2002).

## Additional immunohistochemistry

Immunohistochemistry was performed using PI3K (1:200, Santa Cruz Inc., Santa Cruz, CA), PKB/Akt [1:200, anti-protein kinase B (Akt), Stressgen, Victoria, Canada], pAkt [1:200, anti-phospho-Akt (Ser473), Cell Signaling Technologies, Danvers, MA] and the nuclear signalling transcription factor NFkB p65 subunit (1:200, anti-NFkB p65, Santa Cruz, Santa Cruz, CA) and p50 subunit (1:200, anti-NFkB p50, Santa Cruz, Santa Cruz, CA). For synaptic identification, anti-synaptophysin (1:200, Santa Cruz, Santa Cruz, CA, USA, polyclonal) and Anti-Choline Acetyltransferase (ChAT) (1:100, Abcam, Cambridge, UK, polyclonal) were used. Identification of IR and insulin was performed with immunohistochemistry using antibodies to IRβ (C-19) (1:100, Santa Cruz Biotechnology Inc., Santa Cruz, CA, USA).

Tissue specimens were examined under fluorescence microscopy (Zeiss Axioskope, Axiovision and Axiocam, Zeiss Canada, Toronto, Canada) at 400× and images obtained were examined based upon brain regions of interest sectioned at 10 μm (Appendix 1). Calculation of the number of immunofluorescent profiles as well as the relative luminosity was performed using Adobe Photoshop (Adobe Photoshop 9.0, Adobe, San Jose, CA, 2005). In grey matter regions, the total numbers of neurons per transverse section, as well as the numbers of neurons with positive immunolabelling for the above markers, and their potential nuclear activation, were recorded. Luminosity was classified as none-low (luminosity value of 0–150), moderate (150–250) or high (>250) using Adobe Photoshop software (scale of 0–255 with arbitrary units). An additional measurement of neuronal nuclear immunolabelling for pAkt and NFκB was also performed using a pre-determined luminosity measurement threshold of 150 (no units), below which negative nuclear reactivity was assigned for both neurons and glia. All measurements were performed by a single examiner blinded to the group identity. For synaptic presence, cortical sections immunostained with synaptophysin and ChAT were examined with densitometry using Image-Pro Plus image analysis (Media Cybemetics). A total of 25 randomly chosen areas of cortex, thalamus, and hippocampus from 10 animals per cohort group were examined at 400×.

## Electrophoretic mobility shift assays

For evaluation of CREB binding to DNA, brain tissue was obtained and placed in Totex buffer (20 mM HEPES pH 7.9, 350 mM NaCl, 20% glycerol, 1% igepal, 1 mM $MgCl_2$, 0.5 mM EDTA, 0.1 mM EGTA, 0.1 mM PMSF, 5 μg/ml aprotinin, 50 μM DTT), followed by cell lysis on ice for 30 min, centrifugation at 14 000 r.p.m. for 15 min at 4°C, with supernatant retained. Protein levels were determined by the Bradford method (Biorad) and samples stored at −80°C. Equal amounts of protein were incubated in a 20-μl reaction mixture containing 20 μg of bovine serum albumin; 1 μg of poly (dI–dC); 2 μl of buffer containing 20% glycerol, 100 mM KCl, 0.5 mM EDTA, 0.25% NP-40, 2 mM dithiothreitol, 0.1% phenylmethylsulphonyl fluoride and 20 mM HEPES, at pH 7.9; 4 μl of buffer containing 20% Ficoll 400, 300 mM KCl, 10 mM dithiothreitol, 0.1% phenylmethylsulphonyl fluoride and 100 mM HEPES, pH 7.9; and 20 000–50 000 c.p.m. of 32P-labelled oligonucleotide (S) corresponding to a CREB-binding site (5′-CAA TGA CAT GCG GCT ACG TCA CGG CGC AGT GCC C-3′). After 20 min at room temperature, reaction products were separated on a 12% non-denaturing polyacrylamide gel. Radioactivity of dried gels was detected by exposure to Kodak X-Omat film, and images on the developed film were scanned into a computer using a UMAX 1200s scanner. Densitometry was performed using Scion Image software (Scion Corp., Frederick, MD).

For evaluation of NFκB binding to DNA, nuclear proteins were extracted with NE-PERTM Nuclear and Cytoplasmic Extraction Reagents (Pierce, Rockford, IL). Protein–DNA complexes were detected using biotin end-labelled double-stranded DNA probes prepared with the Biotin 3′ End DNA Labeling Kit (Pierce). The binding probe used was 5′-TCGACAGA[GGG**A**CT**TT**CC]GAGA GGC-3′, with the binding site indicated in square brackets, and bold letters indicating regions of variable nucleotides. Electrophoretic mobility shift assay (EMSA) was performed with a LightShift Chemiluminescent EMSA Kit (Pierce). Briefly, nuclear extracts (10 μg protein) and the 10 × binding buffer with 2.5% glycerol, 5 mM $MgCl_2$, 50 ng/μl poly(dI-dC), 0.05% NP-40, 1 mM DTT and 20 fmol biotin 3′-end labelled double-stranded oligonucleotide were incubated at room temperature for 1 h in a volume of 20 μl. For NFκB supershift analysis, an anti–NFκBp65 polyclonal antibody (Santa Cruz; 1 μg per reaction) was incubated with the nuclear proteins on ice for 1 h before labelled oligonucleotide was added. Reaction products were separated by electrophoresis [5% acrylamide (29:1 acryl/bis)] in 0.5 × TBE. After electrophoresis, the protein–DNA complexes were transferred onto nylon membranes and detected using chemiluminescence (LightShift kit; Pierce).

## Analysis

All statistical comparisons were intended between the following groups: D I-I and D S-I; D I-I and D I-S; D I-I and C I-I; D S-I and D S-S; D S-I and C S-I; C I-I and C S-I; C I-I and C I-S; and C S-I and C S-S. Comparison testing was not performed between other grouped cohorts, with Bonferroni corrections applied as appropriate for the above group comparisons.

Data collected in the groups were expressed as mean ± standard error. One-way matched/unmatched ANOVA and Student's *t*-tests were performed to compare means between diabetic and control groups. The Repeated Measures ANOVA assessment was performed for data obtained during the four cognitive studies, as individual scoring during 1 week partially depended upon

performance of the prior week, with the D I-I group compared to the D S-I and D I-S groups, and the D S-I group compared to the D I-S and D S-S groups. Also, Area Under The Curve statistical testing was performed for cognitive testing other than object recognition tasks. Again, only the groups intended to have statistical comparisons were analysed as such. For the purposes of molecular studies and comparisons, one control (non-diabetic) group was used as a control value, with subsequent comparisons to other diabetic groups for the molecular test studied.

## Results

### Intranasal insulin delivery quantification

Quantification of radiolabelled insulin delivery identified peak delivery to the brain within 1 h after I-I delivery and around 6 h with S-I. Systemic insulin concentrations with intranasal delivery were limited as compared with subcutaneous delivery (Fig. 1). Mice receiving I-I treatment did not suffer adverse effects throughout the 1-, 2- and 6-h monitoring periods before sacrifice. S-I delivery led to much higher concentrations of whole blood insulin and development of hypoglycaemia-induced illness in approximately one-third of mice. Hepatic and kidney insulin levels were overall two to three times higher in mice administered S-I.

### Diabetes

After STZ injection, mice developed diabetes within 2 weeks in 262/304 (86%) of animals. Diabetic mice were smaller than non-diabetic mice throughout life beginning 1 month after STZ injection (Table 1), with D I-I mice maintaining weight better than D I-S mice. Hyperglycaemia was identical in D I-I or D I-S mice, but D S-I mice had less hyperglycaemia and developed hypoglycaemia associated with mortality in some instances. Non-diabetic (C) S-I mice also had increased mortality levels relative to C S-S or C I-I mice (Table 1). Mouse glycated haemoglobin levels were increased in all diabetic mice at 9 months of life, and were identical between I-I and I-S mice, but reduced in S-I mice. The mortality rate in diabetic mice was significantly higher than in non-diabetic mice, although mice receiving I-I had improved mortality relative to I-S, S-S and S-I mice (Table 1) (Kaplan–Meier survival statistics).

The second cohort groups used to complete data within each intervention group consisted of four mice in each of the C S-I, D S-S, D S-I, D I-S and D I-I groups. This led to a data with a minimum of eight mice in each intervention group ($n = 9$ D I-I, $n = 10$ D I-S, $n = 9$ D S-I, $n = 10$ D S-S, $n = 8$ C I-I, $n = 11$ C S-I, $n = 8$ C S-S, $n = 8$ C I-S).

### Cognitive behavioural data

Cognitive testing continued until 33 weeks of diabetes. All cognitive data was based upon a minimum of eight mice in each cohort group at all time points. Learning processes for each of the tasks appeared to be similar between diabetic and non-diabetic mice over the first several weeks (Fig. 2). Diabetic mice performed better than non-diabetic mice in the first weeks of the Radial Arm Test, as demonstrated previously (Toth *et al.*, 2006), hypothesized to be due to hyperphagia contributing to greater exploratory behaviour. In general, diabetic mice demonstrated waning performances on each of the behavioural tasks after 7–10 weeks of diabetes, with impaired performances continuing throughout the remainder of the 33 weeks of testing. Both D I-I and D S-I mice performed better than diabetic cohorts (D I-S and D S-S) in the Morris Water Maze, Holeboard Test and Radial Arm Test tasks (Fig. 2), although D I-I mice consistently outperformed D S-I mice, particularly in the Morris Water-Maze task. In the Morris Water Maze, diabetic mice also spent less time in the hemisphere of the hidden platform (target zone) than non-diabetic mice, although D I-I mice continued to spend time in the target zone similar to that of the non-diabetic mice (Supplementary Fig. 1). Mistakes made in either of the Holeboard or Radial Arm Tests were also magnified with diabetes and increased with duration of diabetes, although D I-I mice made similar numbers of mistakes as non-diabetic mice (Supplementary Fig. 1). Mouse performance in the Object Recognition task demonstrated novelty-seeking behaviour in control mice and D I-I mice, but not in other diabetic cohort groups (Fig. 2, Supplementary Fig. 1). Additional assessments using the Area Under the Curve for each intervention cohort revealed statistically different performances on cognitive testing as described in the figure legends. Analysis provided by the Repeated Measures ANOVA testing revealed early and late time points for differences in intervention groups, as demonstrated in Fig. 2 and Supplementary Fig. 1.

Taken together, these behavioural experiments demonstrated better maintenance of visuospatial, procedural and objection recognition memory functioning in the diabetes-exposed brain receiving intranasal insulin as compared to the diabetic mouse brain not receiving intranasal insulin.

### MRI and brain weight data

Volumetric measurements of brain demonstrated diffuse cerebral atrophy after 5 months of diabetes (Fig. 3), with protection demonstrated in D I-I mice after 8 months of diabetes. Although not identified within individual brain regions at earlier time points, diabetes-associated atrophy was detected in the sensorimotor cortex, caudate/putamen, corpus callosum, internal capsule, CA3 portion of hippocampus and cerebral peduncle (Fig. 3) after 8 months of diabetes. In each of these brain regions, D I-I mice had measurable protection from atrophy (Fig. 3). Measurement of brain mass showed evidence of brain atrophy after 5 months of diabetes, with protection against loss of brain mass first detected in D I-I mice at 8 months of diabetes (Fig. 3).

As found previously (Toth *et al.*, 2006), there were no changes in MR $T_1$ or perfusion-weighted imaging measurements identified. Although initial changes could be seen after 5 months, evidence of diabetes-associated leukoencephalopathy

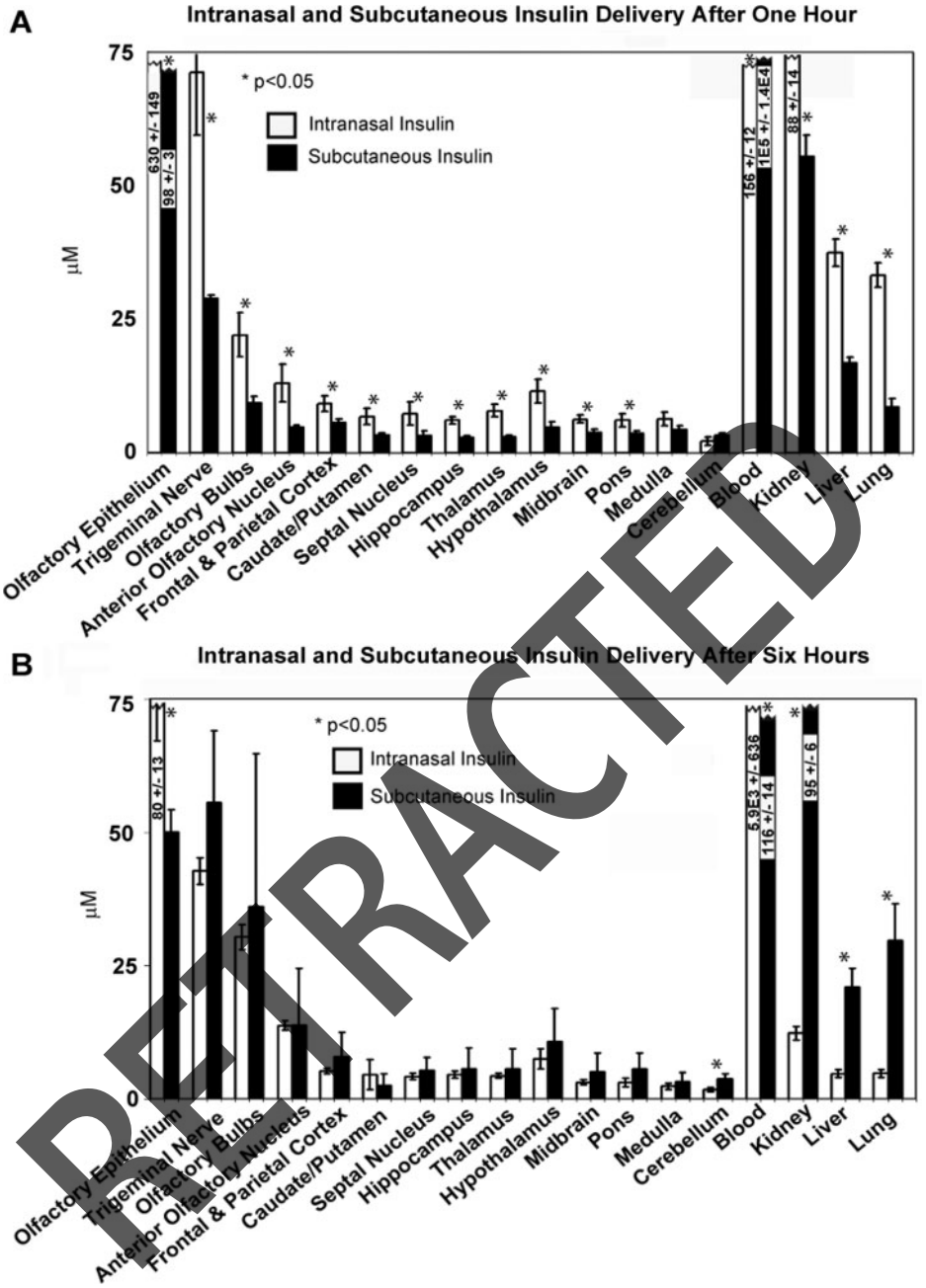




**Fig. 1** Radiolabelled insulin detection. After 1 and 6 h of either I-I (open bars) or S-I (closed bars), I-I led to more rapid and elevated insulin presence in central nervous system structures, including at cortex and deep brain structures, with much less insulin detected in blood than with S-I (**A**). At 6 h after delivery (**B**), intranasal insulin amounts rose in blood, and subcutaneously delivered insulin had slowly penetrated nervous system structures, albeit at lesser amounts than with earlier arrival of intranasally delivered insulin. Significant differences were determined by matched *t*-tests, with asterisk indicating significant difference ($P < 0.05$) between the intranasal and subcutaneous insulin delivery techniques for each tissue ($n = 4$ mice in each mouse cohort for each time point).

was more easily detected after 8 months of diabetes in all diabetic mice using quantitative $T_2$ map values. Although D I-I mice were protected from heightened $T_2$ map values after 8 months, there were still diabetes-mediated WMA present in numerous regions of brain described as white matter regions including corpus callosum and internal capsule, while similar $T_2$ changes could be identified in grey matter regions, such as cortex and hippocampus (Fig. 3). These changes were heterogenous, and were not identified in other brain regions of interest (Appendix 1).

## White matter analysis

Quantitative evaluations of histological sections were performed to determine myelin presence in brain regions of interest (Appendix 1). Both LFB preparations and MBP

**Table 1** Murine weights, fasting glycaemia levels, glycated haemoglobin levels and survival numbers at induction of diabetes and at harvesting at months 1, 3, 5 and 8 of diabetes

| Timepoint | Prior to injection of STZ/carrier | Month 1 | Month 3 | Month 5 | Month 8 |
|---|---|---|---|---|---|
| Murine weight | (g ± SEM) | (g ± SEM) | (g ± SEM) | (g ± SEM) | (g ± SEM) |
| Non-diabetic S-S mice | 25.6 ± 3.2 (*n* = 25) | 32.7 ± 3.8 (*n* = 25) | 39.7 ± 4.0 (*n* = 24) | **43.4 ± 4.3**$^{*}$ **(*n* = 24)** | **47.2 ± 4.9**$^{*}$ **(*n* = 23)** |
| Non-diabetic S-I mice | 25.8 ± 3.9 (*n* = 25) | 30.4 ± 4.1 (*n* = 20) | 34.6 ± 4.7 (*n* = 17) | **36.2 ± 5.1**$^{*}$ **(*n* = 15)** | **37.0 ± 5.4**$^{*}$ **(*n* = 12)** |
| Non-diabetic I-S mice | 25.1 ± 3.7 (*n* = 25) | 32.1 ± 3.9 (*n* = 25) | 40.1 ± 4.2 (*n* = 25) | 44.7 ± 4.6 (*n* = 25) | 48.1 ± 5.2 (*n* = 24) |
| Non-diabetic I-I mice | 25.4 ± 3.3 (*n* = 25) | 31.9 ± 3.5 (*n* = 24) | 36.2 ± 4.9 (*n* = 23) | 39.1 ± 5.3 (*n* = 22) | 43.4 ± 4.8 (*n* = 21) |
| Diabetic S-S mice | 25.2 ± 3.3 (*n* = 40) | 26.9 ± 4.2 (*n* = 34) (3 non-diabetic) | 28.4 ± 4.3 (*n* = 30) | 30.6 ± 5.7 (*n* = 20) | 31.5 ± 5.8 (*n* = 16) |
| Diabetic S-I mice | 25.4 ± 3.4 (*n* = 40) | 26.4 ± 4.8 (*n* = 31) (2 non-diabetic) | 27.2 ± 3.8 (*n* = 24) | 28.2 ± 4.1 (*n* = 16) | 28.8 ± 4.9 (*n* = 12) |
| Diabetic I-S mice | 25.2 ± 3.4 (*n* = 40) | 26.2 ± 4.8 (*n* = 33) (3 non-diabetic) | 28.9 ± 4.2 (*n* = 30) | 30.2 ± 4.9 (*n* = 22) | **30.4 ± 5.2**$^{\&}$ **(*n* = 18)** |
| Diabetic I-I mice | 25.6 ± 3.5 (*n* = 40) | 27.8 ± 4.0 (*n* = 36) (3 non-diabetic) | 30.9 ± 4.5 (*n* = 35) | 34.8 ± 3.6 (*n* = 33) | **35.6 ± 4.9**$^{\&}$ **(*n* = 30)** |
| Murine glycaemia and 8 month glycated haemoglobin | (mmol/l) | (mmol/l) | (mmol/l) | (mmol/l) | (mmol/l) (percentage of haemoglobin) |
| Non-diabetic S-S mice | 5.5 ± 2.3 | 5.9 ± 2.6 | 6.1 ± 2.7 | 6.2 ± 3.0 | **6.6 ± 3.2**$^{*}$ ***(12.4% ± 4.8%)*** |
| Non-diabetic S-I mice | 5.4 ± 2.6 | 3.5 ± 2.7 | 3.9 ± 2.9 | 4.1 ± 3.0 | **4.0 ± 3.1**$^{*\ \delta}$ ***(9.2% ± 4.1%)*** |
| Non-diabetic I-S mice | 6.0 ± 2.8 | 5.9 ± 2.6 | 5.9 ± 2.8 | 6.1 ± 3.1 | 6.3 ± 2.7 *(12.1% ± 4.7%)* |
| Non-diabetic I-I mice | 5.8 ± 2.6 | 5.7 ± 2.9 | 5.6 ± 3.0 | 5.7 ± 3.0 | 5.7 ± 3.2 *(12.6% ± 4.9%)* |
| Diabetic S-S mice | 5.7 ± 2.7 | 31.7 ± 4.9 | 32.3 ± 6.1 | 32.2 ± 6.2 | **32.4 ± 6.0 *(31.6% ± 6.2%)***$^{\&}$ |
| Diabetic S-I mice | 5.6 ± 2.6 | 24.7 ± 5.2 | 25.9 ± 5.8 | 24.3 ± 5.6 | **24.8 ± 6.1 *(24.1% ± 6.6%)***$^{\&}$ |
| Diabetic I-S mice | 6.1 ± 2.9 | 32.2 ± 4.6 | 32.1 ± 5.3 | 32.1 ± 5.2 | 32.3 ± 5.8 *(32.0% ± 6.0%)* |
| Diabetic I-I mice | 5.8 ± 2.8 | 31.5 ± 4.5 | 31.6 ± 5.0 | 31.6 ± 5.2 | 32.0 ± 5.6 *(30.2% ± 6.4%)* |
| Murine survival numbers | Number of mice | Number of mice | Number of mice | Number of mice | Number of mice |
| Non-diabetic S-S mice | 25/25 (100%) | 25/25 (100%) | 24/25 (960%) | 24/25 (96%) | **23/25 (92%)**$^{*}$ |
| Non-diabetic S-I mice | 25/25 (100%) | 20/25 (80%) | 17/25 (68%) | 15/25 (60%) | **12/25 (48%)**$^{*\ \delta}$ |
| Non-diabetic I-S mice | 25/25 (100%) | 25/25 (100%) | 25/25 (100%) | 25/25 (100%) | 24/25 (96%) |
| Non-diabetic I-I mice | 25/25 (100%) | 24/25 (96%) | 23/25 (92%) | 22/25 (88%) | 21/25 (84%) |
| Diabetic S-S mice | 40 (100%) | 34/37 (3 non-diabetic, 92%) | 30/37 (81%) | 20/37 (54%) | 16/37 (43%) |
| Diabetic S-I mice | 40 (100%) | 31/38 (2 non-diabetic, 82%) | 24/38 (63%) | 16/38 (42%) | 12/38 (32%) |
| Diabetic I-S mice | 40 (100%) | 33/36 (3 non-diabetic, 92%) | 30/36 (83%) | 22/36 (61%) | **18/36 (50%)**$^{\&}$ |
| Diabetic I-I mice | 40 (100%) | 36/39 (3 non-diabetic, 92%) | 35/39 (90%) | 33/39 (85%) | **30/39 (77%)**$^{\&\ \Phi}$ |

Glycated haemoglobin values are presented in italics in the 8 month column for glycemia levels. For murine survival, Kaplan–Meier statistics were performed between cohort groups. All measures are mean ± SEM for weights, glycemia levels and glycated haemoglobin levels. $^{*}$Indicates significance at $P < 0.05$ with comparison of non-diabetic S-S and S-I mice cohort groups; $^{\&}$Indicates significance between diabetic cohort groups receiving I-S and I-I; $^{\Phi}$Indicates significance with comparison of diabetic I-I mice to S-S and I-S diabetic cohort groups; $^{\delta}$Indicates significance with comparison of non-diabetic S-I mice to all other non-diabetic mice using multiple ANOVA testing with Bonferroni *post hoc* *t*-test comparisons ($\alpha = 0.016$). Bold values indicate statistical significance as indicated by the superscripted symbols.

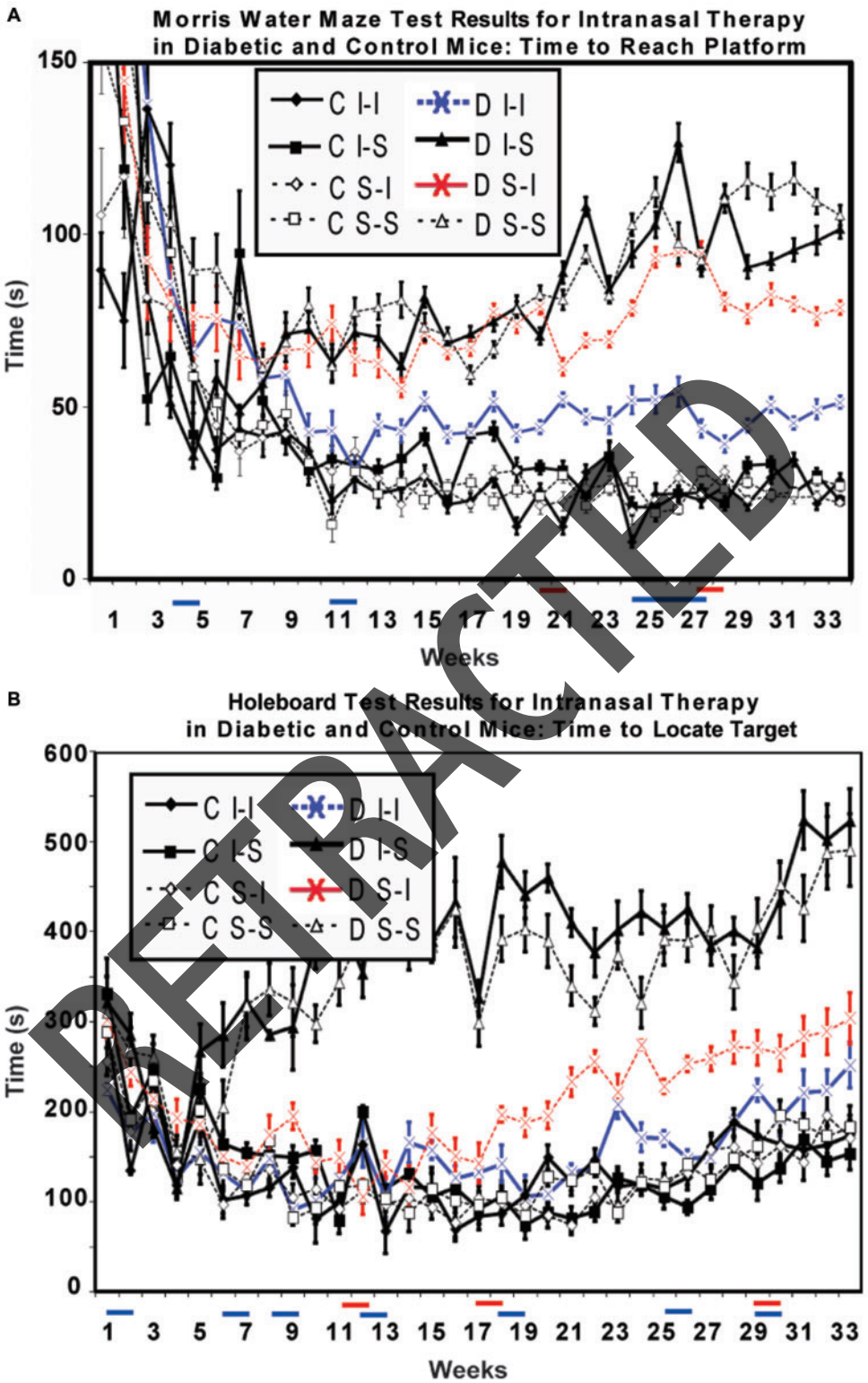






**Fig. 2** Cognitive behavioural data. Mice with diabetes are indicated with a 'D', while mice without diabetes (control mice) are indicated with a 'C'. Delivery of subcutaneous saline is indicated as 'S-S', subcutaneous insulin as 'S-I', intranasal saline as 'I-S' and intranasal insulin as 'I-I'. No baseline differences existed between any of the mouse cohorts. Morris Water-Maze testing demonstrated learning ability in each cohort, regardless of diabetes presence (**A**). Times to reach the platform continued to improve after 7–9 weeks in non-diabetic mice and D I-I mice, whereas the performance of other diabetic mice failed to improve with prolongation of their later times to complete testing. D S-I mice performed better than D S-S or D I-S mice at later time points, while D I-I mice outperformed all other diabetic mice after 9 weeks of time. In the Holeboard test, both D I-I and D S-I mice outperformed other diabetic mouse cohorts after 7 weeks of testing (**B**). In the initial stages of the Radial Arm Test (**C**),

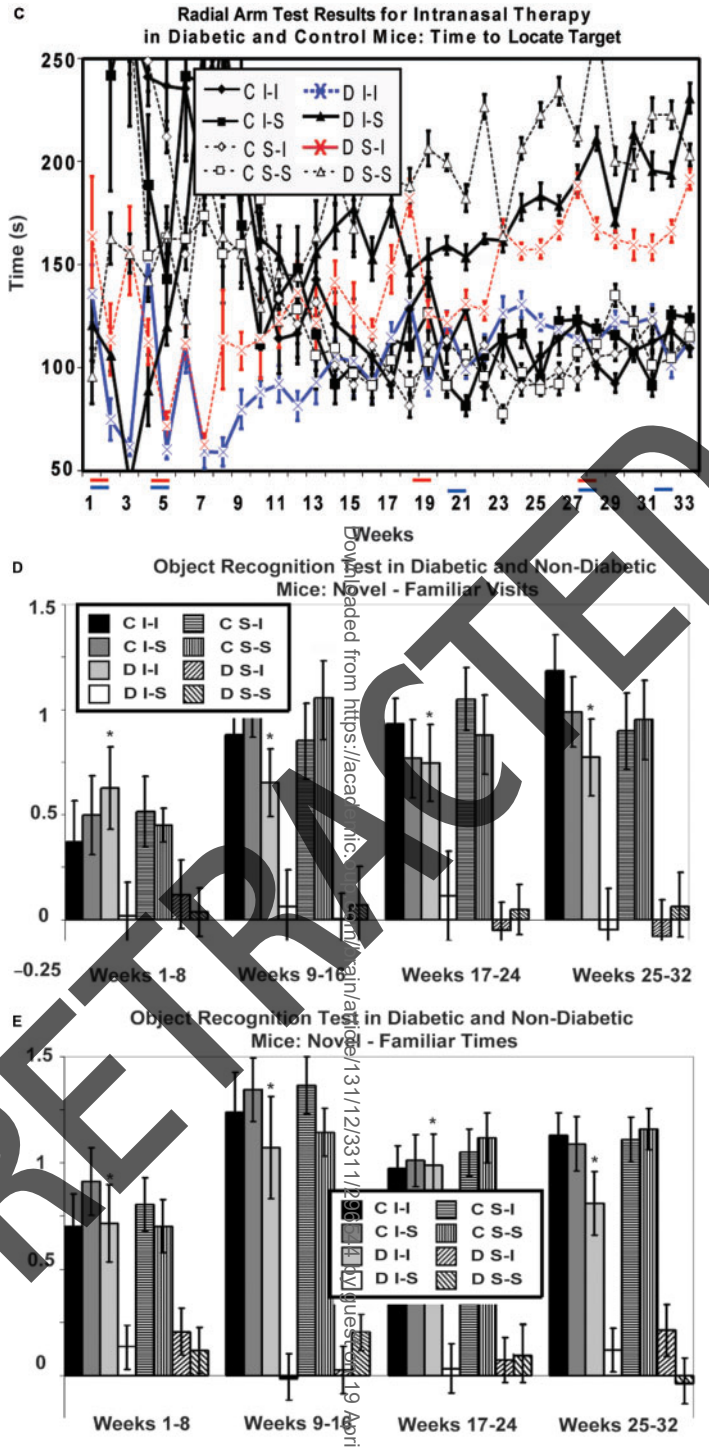






**Fig. 2** Continued

diabetic mice outperformed non-diabetic mice, perhaps due to enhanced search behaviour related to hyperphagia. After 5 weeks, D I-I and D S-I mice found their targets faster than other diabetic mouse cohorts, whose performance diminished further over time. After 22 weeks, D I-I mouse times were improved relative to D S-I times. The Object Recognition Task results are presented as the average of each of 8 consecutive weeks. This task demonstrated less novelty-seeking behaviour in terms of both visits (**D**) and time spent (**E**) at novel objects in the T2 portion of the experiment for D I-S, D S-I and D S-S mouse cohort groups. For **A–C**, Repeated Measures ANOVA testing revealed both early and late time points of significance for D S-I and D I-I mouse cohorts, indicated under the graph with red bars (D S-I) or blue bars (D I-I) for the weeks where significant differences were identified, when compared to D S-S and D I-S mice, or all other diabetic mouse cohorts respectively. For **A–C**, additional Area Under The Curve measurements identified significantly improved performances for D I-I mice compared to the D S-I and D I-S groups ($P < 0.025$ using Bonferroni corrections). For **D** and **E**, significant differences were determined by multiple ANOVA tests, with asterisk indicating significant difference ($P < 0.016$ using Bonferroni corrections) between the D I-I mouse group and other diabetic mouse cohorts ($P < 0.016$ using Bonferroni corrections) for the respective time points ($n = 8–10$ mice in each mouse cohort for each time point).

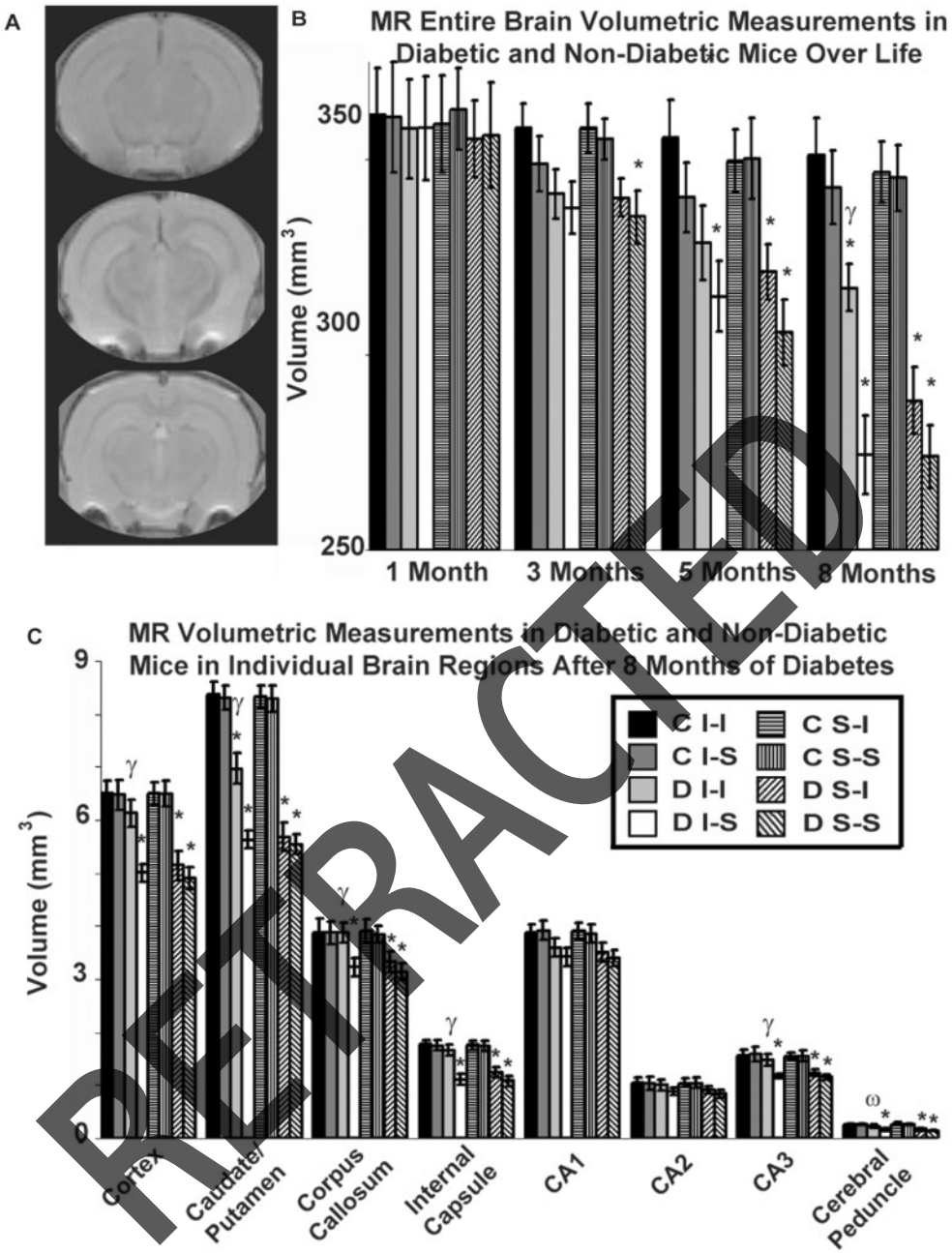




**Fig. 3** MRI data. The diabetic murine brain demonstrated atrophy and development of white matter changes over time. There were no differences between cohort groups for volumetric measurements until after 3 months of diabetes, and no difference between cohort groups for individual brain region volumetric measurements until 5 months of diabetes. Samples of MR $T_2$ images after 8 months of diabetes are demonstrated using aged-matched non-diabetic mouse brain (top), diabetic mouse brain receiving long-term intranasal insulin (middle) and diabetic mouse brain receiving intranasal saline (bottom) (**A**). Volumetric measurements of the entire brain indicated generalized loss of brain volume over time in diabetes, first demonstrable after 3–5 months of diabetes (**B**). D I-I mice were protected from cerebral atrophy when compared to other diabetic mouse cohorts, detectable after 8 months of diabetes. Individual brain regions also showed atrophy after 8 months of diabetes in diabetic mouse cohort groups other than D I-I mice (**C**). Wet brain mass paralleled MRI volumetric measurements, again demonstrating cerebral atrophy in diabetic mice after 5 months, with partial protection found in D I-I mice (**D**). MR $T_2$ map values were significantly elevated in both white and grey matter regions for diabetic mice, with D I-I mice again protected when compared to their diabetic cohort groups (**E**). Significant differences were determined by multiple ANOVA tests, with asterisk (*) indicating significant difference ($P < 0.0125$ using Bonferroni corrections) between the indicated mouse group and other non-diabetic mouse cohorts, while $\omega$ indicates a significant difference ($P < 0.0125$ using Bonferroni corrections) between the D I-I mouse group and the D I-S and D S-S cohort groups for the respective time points. Finally, $\gamma$ indicates a significant difference ($P < 0.0125$ using Bonferroni corrections) between the D I-I mouse group and all other diabetic mouse cohort groups for the respective time points ($n = 4$-6 mice in each mouse cohort for each time point).

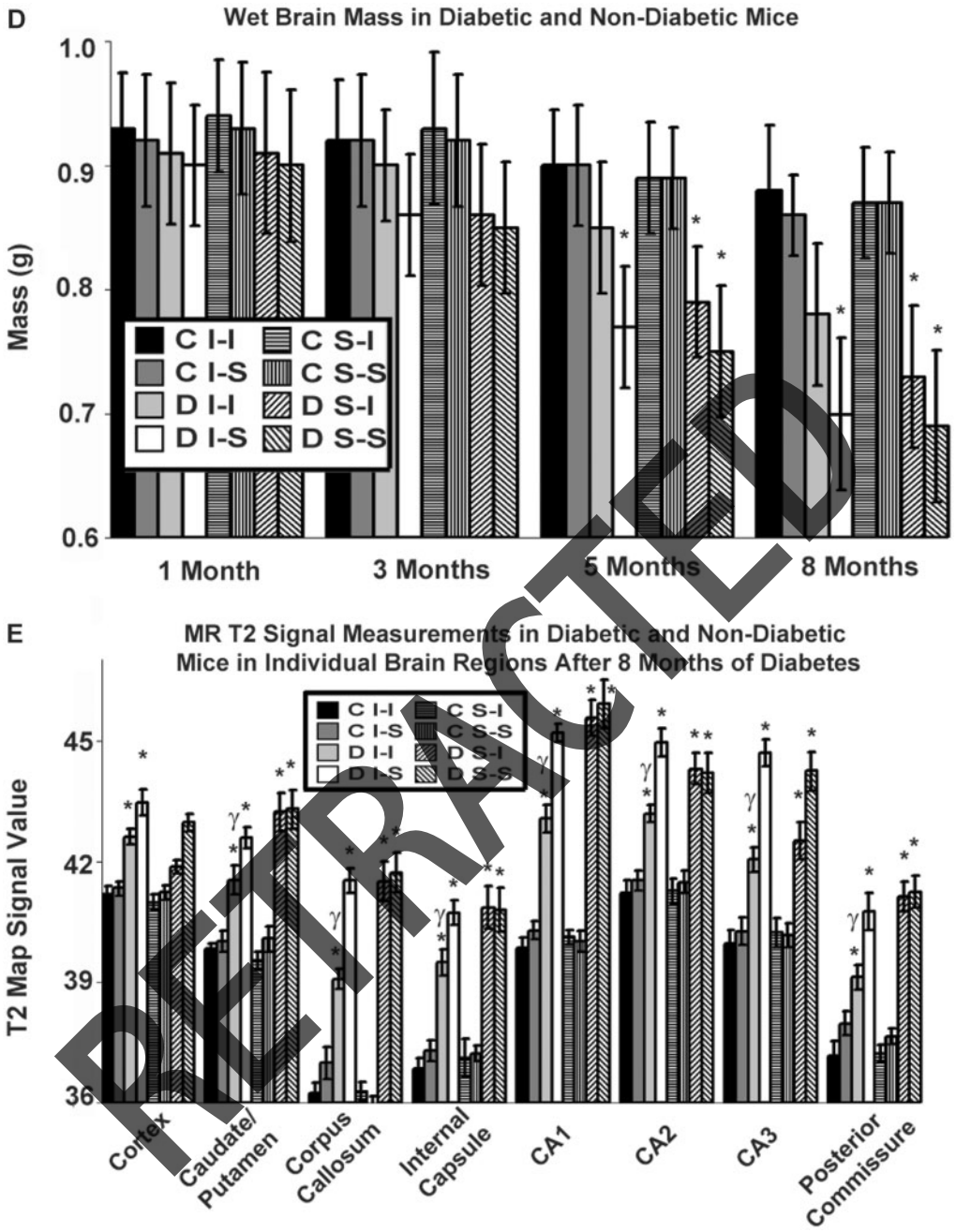


**Fig. 3** Continued.

immunohistochemistry detected reductions in myelin quantity within a number of brain regions of interest (Fig. 4). As determined previously (Toth *et al.*, 2006), none of the identified WMA had a pattern which could be attributed to large vessel infarction. Lost MBP expression closely resembled abnormalities also identified with LFB staining and with $T_2$ measurement changes found with MR imaging (Fig. 4).

As identified previously (Toth *et al.*, 2006), there were no differences in neuronal density over grey matter regions of interest after detailed stereological counts. For example, neuronal densities within the CA1 region of hippocampus were $1.73 \times 10^6/mm^3$ in diabetic mice as compared to $1.79 \times 10^6/mm^3$ in control mice ($P$ = NS). Neuronal densities within other grey matter brain regions (Appendix 1) were similar between diabetic and non-diabetic mouse cohort groups. Oligodendrocyte counts were performed by examination of immunohistochemistry for PDGFRα within both regions of white and grey matter (Appendix 1) and revealed a 44% loss of oligodendrocytes within the internal capsule and corpus callosum regions in D I-S brains as compared to C I-S brains, with oligodendrocyte loss protected in D I-I brains, only demonstrating 17% loss (ANOVA, $P < 0.01$).

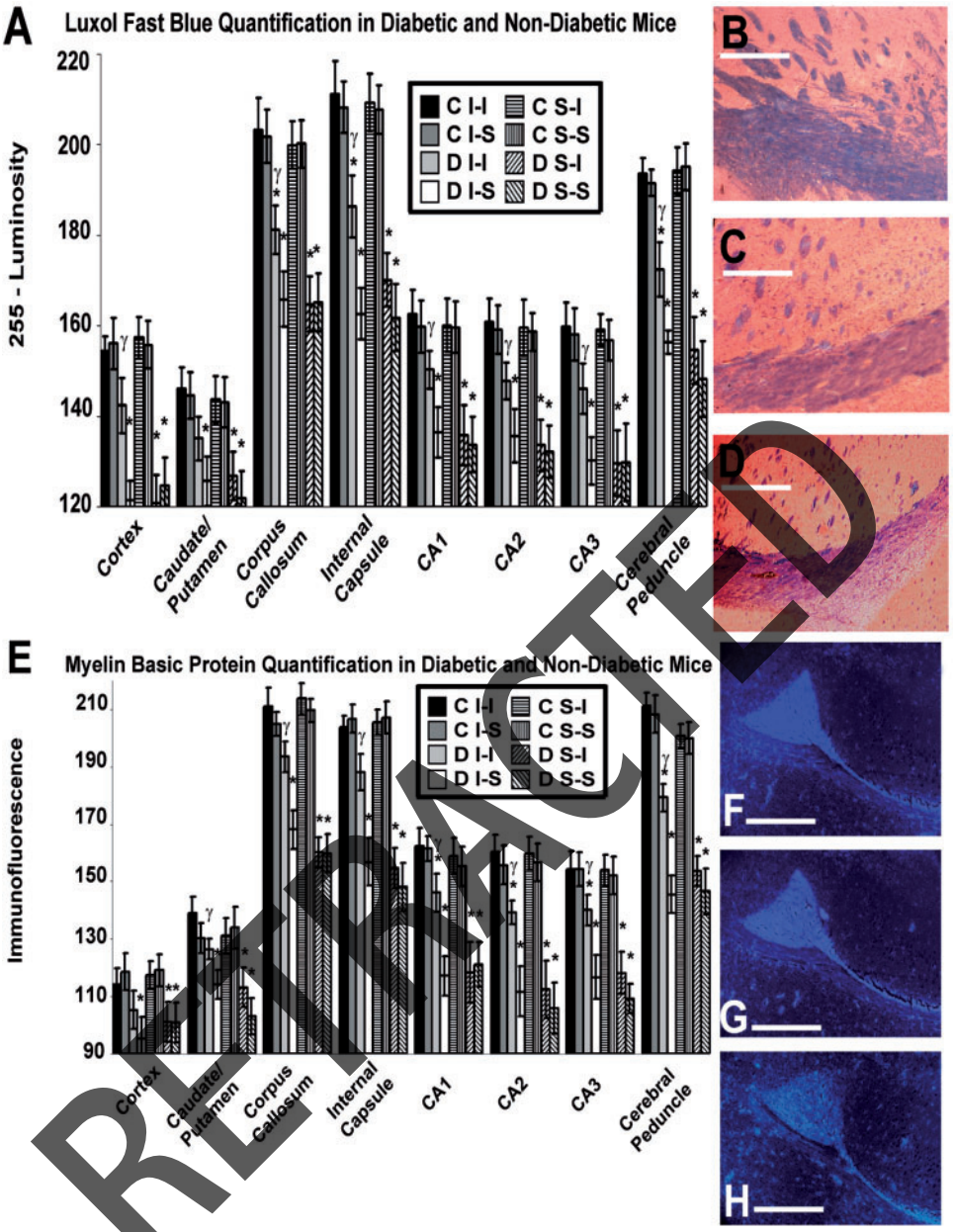




**Fig. 4** Quantification of myelin for both Luxol Fast Blue (LFB) and Myelin Basic Protein (MBP). Data for LFB quantification is demonstrated as (255 − Luminosity), as higher luminosity would indicate greater light passage and therefore, less myelin content. LFB loss occurred in both white and grey matter regions (**A**) of the diabetic murine brain as compared to the non-diabetic brain (C S-S) (**B**), with partial protection present in the D I-I brain (**C**) when compared to the D I-S brain (**D**). (Bars = 20 μm) MBP loss also occurred in both white and grey matter regions (**E**) of the diabetic murine brain as compared to the non-diabetic murine brain (C S-S) (**F**), with partial protection again present in the D I-I brain (**G**) when compared to the D I-S brain (**H**). (Bars = 10 μm) Significant differences were determined by multiple ANOVA tests, with asterisk (∗) indicating significant difference ($P < 0.0125$ using Bonferroni corrections) between the indicated mouse group and other non-diabetic mouse cohorts, while γ indicates a significant difference ($P < 0.0125$ using Bonferroni corrections) between the D I-I mouse group and all other diabetic mouse cohort groups for the respective time points ($n = 4$ mice in each mouse cohort for each time point).

## mRNA and protein quantification

A relative loss of intraneuronal pAkt and decreased nuclear pAkt presence (Fig. 5) was associated with diabetic encephalopathy. Insulin provision, however, led to amelioration of this loss in D S-I mice, and particularly in D I-I mice. Amongst non-diabetic mouse cohorts, there was no significant difference in pAkt presence in either cortical or hippocampal neurons. Quantification of Akt and PI3K mRNA demonstrated downregulation with diabetes in general, while a near return to normal for both PI3K and Akt mRNA levels occurred with I-I delivery in diabetic mice

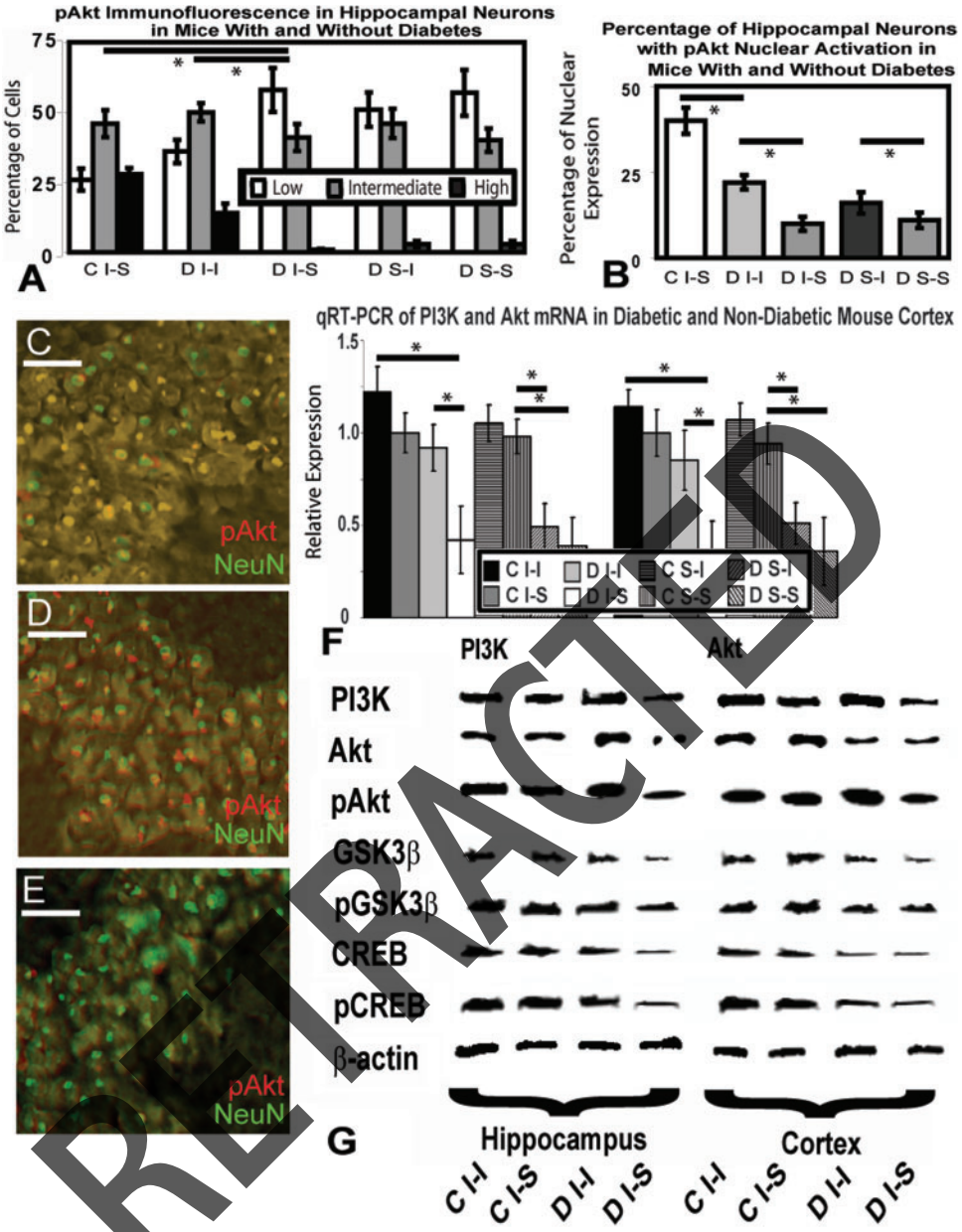




**Fig. 5** The PI3K/Akt pathway is disturbed in the diabetic murine brain. Levels of pAkt fell within hippocampal neurons exposed to diabetes, with partial protection provided in D I-I mice (**A**). Neuronal activation (presence of pAkt in neuronal nuclei) was also diminished in diabetic hippocampal neurons (**B**), with intranasal insulin preventing some of this effect (**B**). Hippocampal neurons in C S-I mice (**C**) demonstrated higher levels of nuclear pAkt presence when compared to D I-I mice (**D**), which were protected when compared to D S-I mice (**E**). (Bars = 25 μm) Both PI3K and Akt mRNA fell in diabetic murine brain tissue from both hippocampus (data not shown) and cortex, (**F**) although D I-I mice were protected against mRNA loss. Similarly, PI3K and Akt protein levels (representative blots, **G**) fell based upon semi-quantitative determination of protein levels in both hippocampus and cortex (**H**). In addition to changes in PI3K and Akt protein loss, similar protein loss is seen for PI3K/Akt pathway proteins including pAkt, GSK3β, pGSK3β, CREB and pCREB (**G,H**). There was no difference in measurements between non-diabetic cohort mouse groups. Quantitative assessment of electrophoretic mobility shift assays (EMSA) (example in **I**) demonstated a loss of CREB DNA binding in diabetic hippocampus, reversed with intranasal insulin provision (**J**). Meanwhile, phosphorylation ratios for Akt, CREB, and GSK3β within hippocampus were increased with I-I provision in diabetic mice (**K**). Quantitative analysis in each situation was performed using three to five samples for each group with multiple ANOVA tests, appropriate Bonferroni corrections, and with asterisk indicating significant difference ($P < 0.016$) between groups indicated by horizontal bars.

(Fig. 5) in cortex (also seen in hippocampus). Protein quantification in the hippocampus and cortex of diabetic mice revealed generalized suppression with diabetes, with partial protection against loss of PI3K, pAkt, GSK3β, pGSK3β and pCREB (no significant difference for Akt and CREB) identified in D I-I mice (Fig. 5). Ratios of phosphorylated to non-phosphorylated downstream markers revealed increased activation (phosphorylation) of Akt

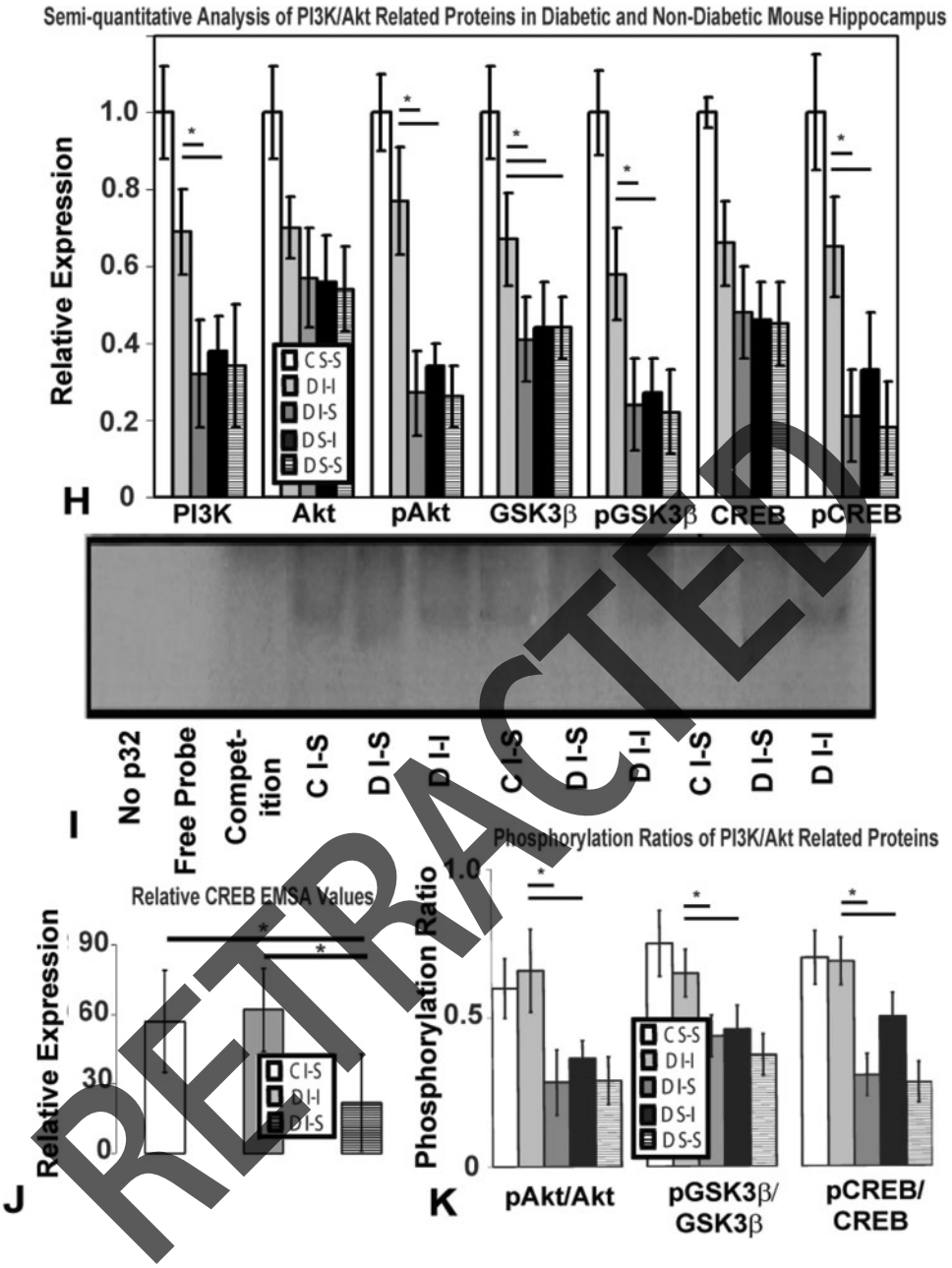


**Fig. 5** Continued.

and CREB, along with increased phosphorylation (inactivation) of GSK3β in the hippocampus for diabetic mice receiving I-I (Fig. 5). EMSAs demonstrated maintained DNA binding for CREB in D I-I mice as compared to D I-S mice (Fig. 5).

Protein and mRNA for portions of the IR, IRβ and IR subsrate (IRS)-1, were also downregulated in the diabetic murine brain except when I-I was provided (Fig. 6). Both IRβ and IRS-1 were expressed over the neurolemma of cortical and hippocampal and cortical neurons, with decreased levels of expression in diabetes, except in D I-I mice (Fig. 6). For non-diabetic mice, intranasal insulin provision also led to elevated IRβ levels (Fig. 6).

Important components of the synaptic complex, the vesicular protein synaptophysin (SYP) and the enzyme choline acetyltransferase (ChAT), were both downregulated in diabetic hippocampus and cortex (Fig. 7). Again, D I-I mice were partially spared from loss of synaptic components within the cerebrum based upon immunofluorescence quantification, protein blotting and qRT-PCR studies (Fig. 7). There were no differences between non-diabetic cohort groups despite the provision of I-I or S-I (Fig. 7), and no loss of synaptic components was demonstrated in the thalamus in any cohort.

Diabetes led to greater accumulation of NFκB and its greater nuclear presence (activation) (Fig. 8). Both neurons

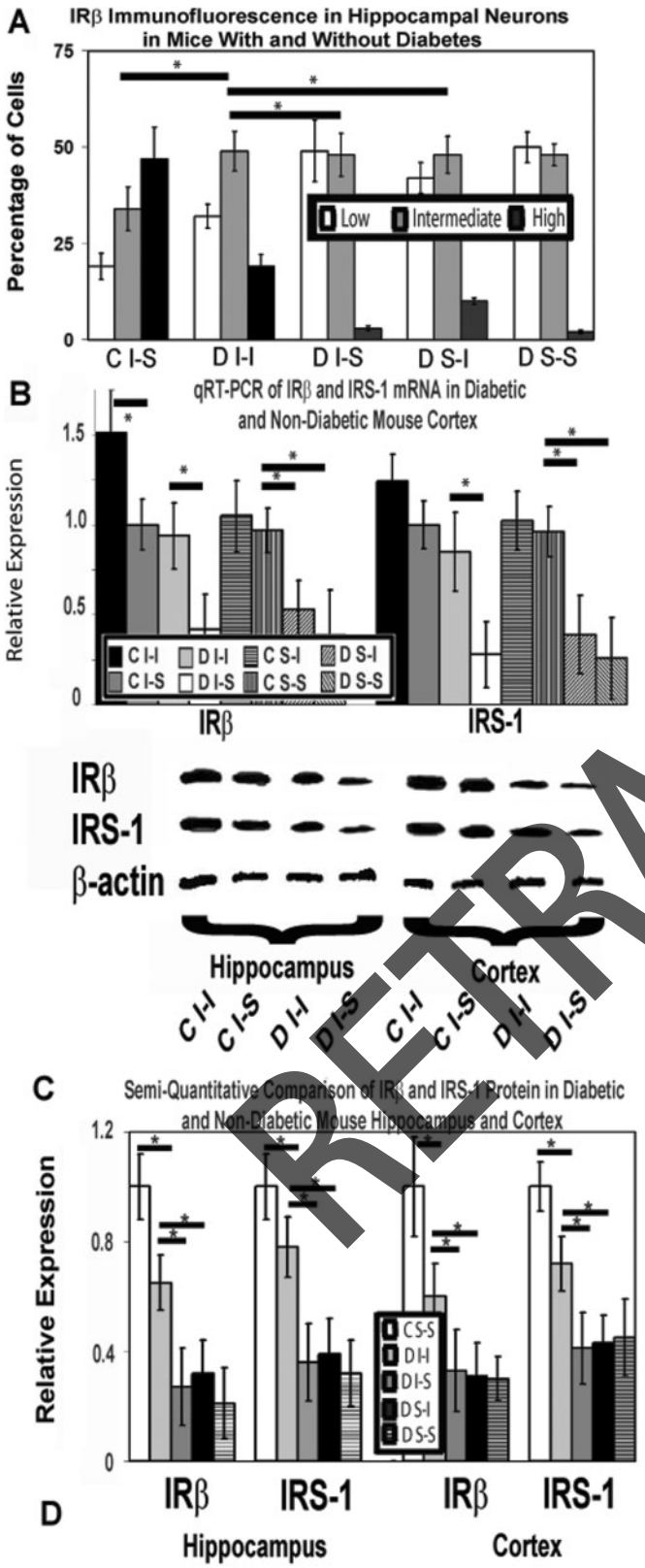


**Fig. 6** Diminution of the insulin pathway in the diabetic murine brain. Levels of IRβ fell within the diabetic murine brain but replenished with I-I, but not S-I (**A**). mRNA for both IRβ and IRS-1 was also deficient in diabetic murine brain regions (hippocampus not shown) such as cortex (**B**). Non-diabetic mice receiving intranasal insulin demonstrated heightened IRβ mRNA, and D I-I mice received protection against loss of both IRβ and IRS-1. Protein levels (**C**) for IRβ and IRS-1 fell in combination with diabetes as demonstrated with quantitative measurements using three protein samples for each group (**D**), with protection again offered by I-I in both the diabetic cortex and hippocampus. There were no differences in measurements between non-diabetic cohort mouse groups. Multiple ANOVA tests, with asterisk indicating significant difference ($P < 0.016$) between groups indicated by horizontal bars, were performed.

and oligodendrocytes in cortical, hippocampal and subcortical regions demonstrated NFκB activation, with suppressed levels of activation demonstrated in D I-I mice. As well, D I-I mice also demonstrated partial suppression of overall NFκB mRNA and protein elevation occurring in both cortex and hippocampus, which exhibited age-dependent increases over time for both diabetic and non-diabetic mice (Fig. 8), but greatest in diabetic mice. Finally, EMSAs demonstrated depressed levels of DNA binding for NFκB in D I-I mice as compared to D I-S mice, but levels remained higher in D I-I mice when compared to non-diabetic mice (Fig. 8). There were no differences in NFκB levels between non-diabetic cohorts.

## Discussion

Intranasal insulin prevented diabetes-mediated cerebral neurodegeneration without leading to prominent systemic effects or modification of glycaemia levels. Replacement of insulin reversed the downregulated PI3K/Akt pathway to slow or diminish the development of brain atrophy, WMA and cognitive decline.

### Systemic and neural effects of subcutaneous and intranasal insulin

Insulin delivered through an intranasal route led to improvements in behavioural (Fig. 2), morphological (Figs 3 and 4), and molecular abnormalities (Figs 5–8) within the diabetes-exposed brain. I-I did not confer the risks of systemic hypoglycaemia identified with S-I delivery in this long-term experimental model. Not only did S-I delivery in either of diabetic or non-diabetic mice lead to greater mortality (Table 1) and higher systemic delivery than I-I (Fig. 1), but failed to improve a number of morphological and molecular deficits identified with diabetic encephalopathy. While subcutaneous delivery of insulin led to improved glycated haemoglobin levels at sacrifice, intranasal insulin delivery did not, suggesting that the beneficial effects of I-I in diabetic mice was not due to effects upon hyperglycaemia, which occurred in the D S-I cohort (Table 1). Whereas systemic insulin enters the brain via a receptor-mediated, saturable form of transport (Woods *et al.*, 2003), I-I directly enters the brain bypassing the blood–brain barrier and travelling by extra-cellular bulk flow transport along olfactory and trigeminal perivascular

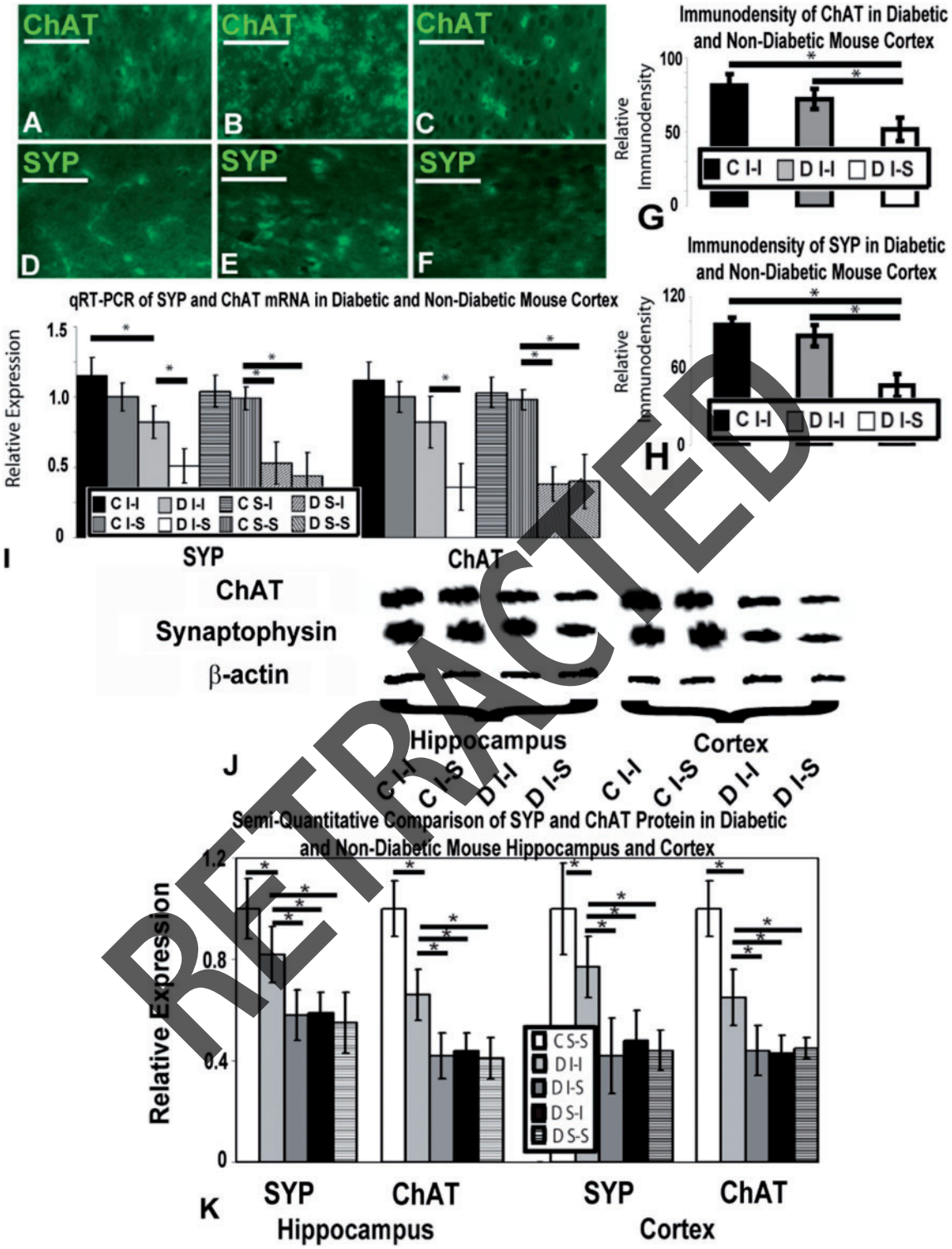




**Fig. 7** Central synaptic components in the diabetic murine brain are decreased. Choline acetyltransferase (ChAT) and synaptophysin (SYP) levels are diminished within the cortex and hippocampus (data not shown) of diabetic mouse brains relative to non-diabetic murine brains (**A, D**). ChAT and SYP levels within the D I-I brain (**B, E**) were not different from that of the C I-S brain (**A, D**), while the D I-S brain demonstrated loss of ChAT and SYP (**C, F**). Losses in synaptic markers were determined by quantification of density for immunostaining for both ChAT (**G**) and SYP (**H**) within cortex and hippocampus (data not shown). qRT-PCR also demonstrated loss of mRNA for both SYP and ChAT (**I**). Finally, quantitative assessment of three protein blots (representative blot, **J**) also portrays a loss of both SYP and ChAT in the hippocampus and cortex of the diabetic murine brain, where protection against synaptic loss is again provided by I-I to the diabetic murine brain (**K**). Multiple ANOVA tests were performed for each comparison, with asterisk indicating significant difference ($P < 0.05$) between groups indicated by horizontal bars.

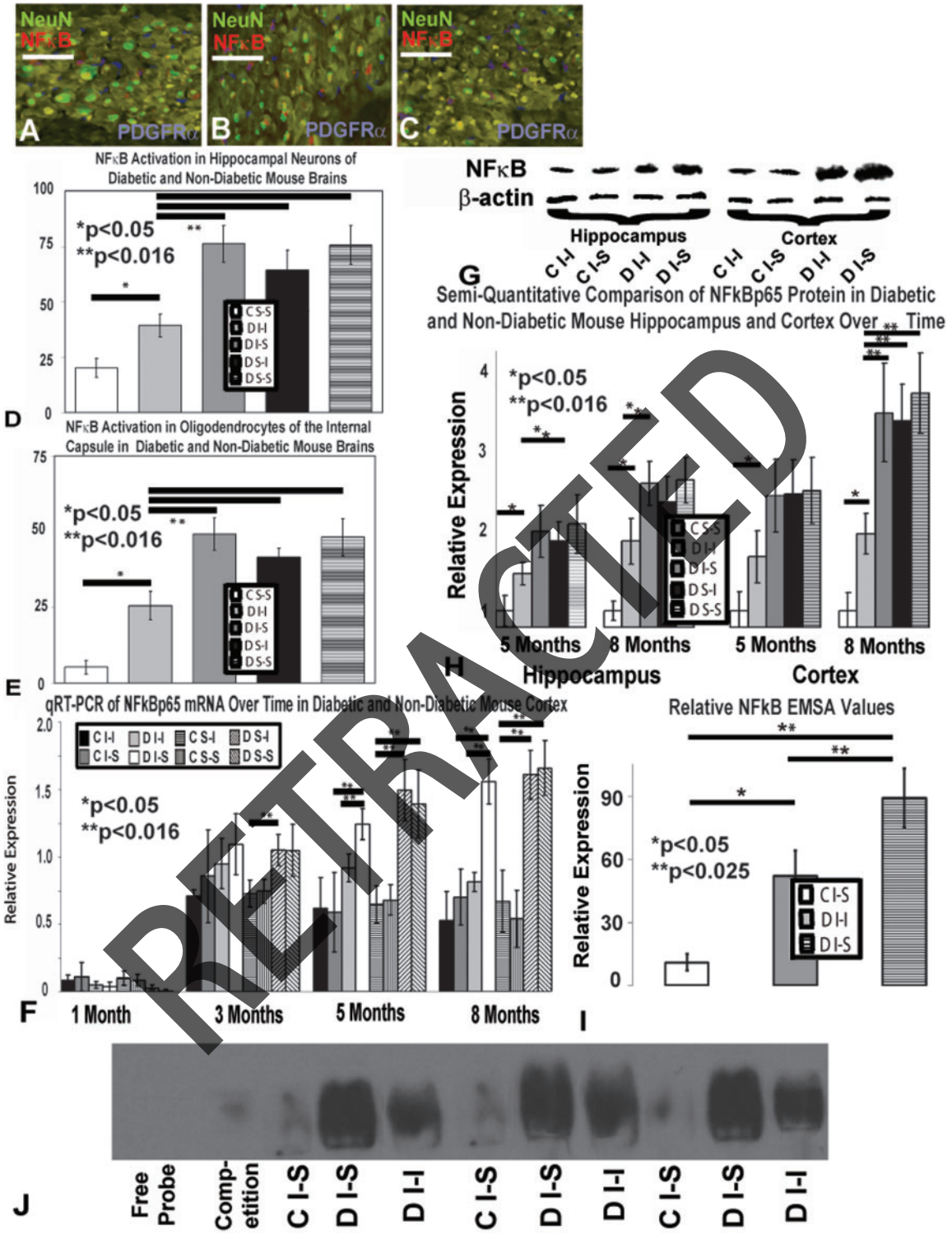






**Fig. 8** Quantification of NFκB expression. Upregulation in diabetic murine brain for NFκB protein and mRNA occurs as compared to non-diabetic brain. In the hippocampus, neurons identified with NeuN and oligodendrocytes, identified with PDGFRα, co-express NFκBp65 least in the C S-S brain (**A**) as compared to diabetic murine brain. D I-I mouse brain (**B**) had less nuclear activation (nuclear presence) than D I-S mouse brain (**C**), within both neurons (**D**) and oligodendroglia (**E**). mRNA measurements of NFκBp65 expression identified age-related increases occurring greatest after 3–5 months of diabetes (**F**), and again ameliorated with I-I. Protein blotting (representative blot, **G**) and its quantitative assessment (**H**) also demonstrated accumulation of NFkBp65 protein over time, accelerated with diabetes, and partially suppressed with I-I. The amount of NFκB binding to DNA was significantly upregulated with diabetes (**I**), with protection from its increase identied in the D I-I cohort, based upon bands obtained from EMSA, an example of which is demonstrated (**J**). Quantitative analysis for Western blots was performed using three samples for each group. For comparisons, multiple ANOVA tests, with asterisk indicating significant difference between groups indicated by horizontal bars, were performed. All diabetic values were significantly less than non-diabetic values (significance not visually demonstrated).

channels, as well as axonal transport pathways (Benedict *et al.*, 2004; Thorne *et al.*, 2004), leading to faster uptake and less systemic insulin presence.

## The role of insulin as a neuroprotective trophic factor

Insulin, a highly conserved peptide that is no longer thought of as solely a promoter of glucose turnover, has now emerged as a key neurotrophic factor in the nervous system alongside and interacting with the IGF-I receptor system, also important in maintaining cognitive function (Trejo *et al.*, 2008). Insulin is a potent trophic factor which becomes lost within type I diabetes. The major site of insulin's activity, IR, is found in high concentration in the brain, particularly in the cerebral cortex, olfactory bulb, hippocampus (Fig. 6), amygdala and septum (Havrankova *et al.*, 1978*a*, *b*; Baskin *et al.*, 1987; Unger *et al.*, 1991). Reduced levels of insulin and its signalling molecules occur in the CSF and brain of Alzheimer disease patients (Craft *et al.*, 1998; Hoyer, 2004). Also, IRs are present at synapses for both astrocytes and neurons (Abbott *et al.*, 1999). As demonstrated in our study, diabetic rodents also demonstrate a loss of insulin transduction machinery (Fig. 6), which has previously been linked to the increased expression of amyloid precursor protein (APP), APP's cleavage enzyme β-secretase, and other abnormalities typical of the Alzheimer disease brain (Ho *et al.*, 2004; Salkovic-Petrisic *et al.*, 2006; Li *et al.*, 2007). It has also been demonstrated that peripheral hyperinsulinaemia and reduced insulin signalling increase levels of amyloid (Aβ) and tau hyperphosphorylation, leading to the formation of both senile plaques and neurofibrillary tangles (Zhao *et al.*, 2004*b*; Freude *et al.*, 2005). In addition, insulin promotes physiologic processes critical for memory, including long-term potentiation, expression of glutamate receptors, and modulation of neurotransmitter levels (Craft and Watson, 2004). Finally, insulin diminishes hypothalamic–pituitary–adrenal-axis activity (Hallschmid *et al.*, 2008), recently speculated to contribute to diabetes-mediated cognitive dysfunction (Stranahan *et al.*, 2008).

## Potentially preventable changes in diabetic encephalopathy

Our experiments have demonstrated that long-term intranasal insulin delivery protected against brain atrophy (Fig. 3). Although other studies have reported evidence of cerebral neuronal loss in diabetes (Li *et al.*, 2007), we could not detect any loss of neuronal density in this experimental diabetic brain model, similar to other recent studies (Stranahan *et al.*, 2008), but we did determine oligodendroglial loss occurs and likely relates to the development of WMA. One potential cause for our detected diabetes-associated brain atrophy (Fig. 3) is the presence of large degree of synaptic loss (Fig. 7), also detected in type II diabetic rat models (Li *et al.*, 2007). Synaptic loss may precede other forms of pathology in some models of Alzheimer disease (Yoshiyama *et al.*, 2007), including neuronal loss. Diabetes also leads to a synergistic potentiation of synaptic loss in transgenic models of Alzheimer disease (Burdo *et al.*, 2008). This may certainly be impacted by the presence of insulin receptor at central synapses (Heidenreich *et al.*, 1983; Matsumoto and Rhoads, 1990; Wan *et al.*, 1997; Zhao *et al.*, 1999). Signal transduction by neuronal IRs is exquisitely sensitive to soluble Aβ oligomer-mediated disruption *in vitro*, and neuronal response to insulin is also inhibited (Zhao *et al.*, 2008). Such synaptic loss identified in our experiments of the diabetic brain may herald subsequent neuronal loss, but other models need to be investigated, and longer duration studies may be necessary to conclude this.

## Insulin's downstream signalling pathways

Insulin is critical for maintenance of numerous downstream intracellular signalling pathways. Insulin stimulation upregulates protein–tyrosine phosphorylation (Mahadev *et al.*, 2004) through downstream activation of IRS-2 (Huang *et al.*, 2005*a*). Insulin presence leads to activation of Akt and phosphorylation of Akt substrates (Fig. 5) (Bruss *et al.*, 2005). In addition, insulin modulates the inner mitochondrial membrane potential through activation of the PI3K pathway, stimulating phosphorylation of Akt and cAMP response element-binding protein CREB (Marshall, 1995; Yao and Cooper, 1995; Fernyhough *et al.*, 2003; Viard *et al.*, 2004; Huang *et al.*, 2005*b*), as well as supporting neuritic extension and branching (Jones *et al.*, 2003). PI3K also enhances voltage-dependent calcium channel current functioning in diabetic neurons (Viard *et al.*, 2004). In our studies, downregulation of PI3K/Akt occurred throughout the diabetic murine brain (Fig. 5), while insulin delivered intranasally, and to a lesser extent, subcutaneously, prevented such downregulation while concurrently leading to improvements in behaviour and morphology.

Insulin's benefits in the diabetic brain may relate to inactivation of GSK-3β and activation of CREB. Besides regulating the transcriptional activities of CREB (Cohen and Frame, 2001; Grimes and Jope, 2001), GSK-3β is also a neuron-specific (Leroy and Brion, 1999) apoptosis promoter in the non-phosphorylated, or active state (Hetman *et al.*, 2000); Akt-mediated phosphorylation of GSK-3β renders it inactive, giving anti-apoptotic properties (Pap and Cooper, 1998; Bijur *et al.*, 2000; Hetman *et al.*, 2000). Similar to insulin in our study, IGF-I also activates the PI3K/Akt pathway (Dudek *et al.*, 1997; Zheng *et al.*, 2002), leading to phosphorylation of CREB and GSK-3β (Leinninger *et al.*, 2004). IGF-I provision also induces oligodendrocyte progenitor proliferation via Akt activation (Cui and Almazan, 2007), with GSK-3β phosphorylation in oligodendrocyte progenitor cells affecting oligodendrocyte stability (Frederick *et al.*, 2007). pGSK-3β may also regulate gene expression and activity of transcriptional factor

binding to the MAG promoter region (Ogata *et al.*, 2004), promoting myelination and possibly explaining insulin-mediated protection against WMA development in the experimental diabetic murine brain (Figs 3 and 4). While CREB phosphorylation inhibits apoptosis in neurons (Walton *et al.*, 1999), the loss of CREB results in impaired axonal growth (Lonze *et al.*, 2002), suggesting that CREB is neuroprotective. Intranasal insulin led to heightened pCREB levels as well as greater CREB DNA binding indicating transcription (Fig. 5). Overall, we hypothesize that insulin's benefits in the diabetic murine brain are due to maintained phosphorylation of CREB and GSK-3β.

## The utility of intranasal delivery in diabetic encephalopathy

In the case of diabetic encephalopathy, and likely the Alzheimer disease brain, insulin's trophic effects are lacking. I-I delivery without modifying systemic glucose or glycated haemoglobin (Table 1) (Tomlinson and Gardiner, 2008) appears to be essential to insulin's long-term benefits in brain exposed to diabetes. Human studies have already demonstrated safe administration of intranasal insulin in patients with Alzheimer disease, leading to some improvement in cognition and modulating markers of Alzheimer disease (Reger *et al.*, 2006, 2008). These studies have concentrated upon the potential benefits of intranasal insulin delivery upon clinical and pathological markers of Alzheimer disease. Other clinical studies examining intranasal insulin delivery have also demonstrated effects upon the CNS, such as improvement in memory (Benedict *et al.*, 2007, 2008), lowering of food intake (Tomlinson *et al.*, 2008), and improvement in mood (Hallschmid *et al.*, 2008). In humans, plasma glucose levels may be minimally impacted by intranasal insulin delivery (Born *et al.*, 2002; Reger *et al.*, 2006, 2008; Tomlinson *et al.*, 2008). As of yet, intranasal insulin delivery to diabetic subjects for the intent of improving memory or other diabetic complications has not yet been described, although intranasal insulin delivery has been examined as a potential method for the treatment of diabetes itself (Owens *et al.*, 2003; Khafagy *et al.*, 2007).

Our study results must be considered under the limitations of working in a murine model, and the inability to achieve a long-term model of murine type I diabetes with optimal glycaemic management as a suitable control group. The mouse cohorts were subjected to intensive testing throughout their lifetime, with the possibility of stressful impacts upon the results obtained. The use of multiple cognitive studies, often needed as part of a battery of tests, may have led to crossover effects affecting results from one cognitive test based upon the preceding test. It is also possible that hypoglycaemia may have impacted some of the results of cognitive testing, and the impact of hypoglycaemia upon the D I-S and C I-S cohort groups was anticipated, but difficult to avoid. As well, performance of behavioural testing within multiple cohorts of mice within each intervention group may have contributed to performance disparities. Based upon our studies, it is difficult to develop a more appropriate control group of diabetic mice with long-term glycaemic control based upon the STZ-induced diabetic model. Despite these difficulties, D S-I mice performed better than D S-S cohort mice during portions of cognitive testing. Although cognitive changes in our mice also seem to occur mainly during the younger and older age time points (similar to expected changes in type I diabetic patients), explanations for a relative plateau of function during the middle-aged years are unknown. (Wessels *et al.*, 2007, 2008; Biessels *et al.*, 2008; Kloppenborg *et al.*, 2008;) At this time, our results are limited to murine models of type I diabetes, and other forms of diabetes, including models of type II diabetes, will need study in the future to confirm our results in other models of diabetes.

## Conclusions

Intranasal insulin delivery is a potential therapy to ameliorate behavioural, morphological and molecular changes occurring in brain exposed to diabetes over time. Our results provide strong evidence for benefits of insulin without impact upon serum glucose levels, indicating that insulin is an important neurotrophic factor in the management of diabetes-mediated brain disease. These data support the development of clinical studies for the prevention and slowing of the adverse effects of diabetes upon the brain using intranasal delivery of insulin.

## Supplementary material

Supplementary material is available at *Brain* online.

## Funding

This study was supported by an operating grant from the Alberta Heritage Foundation for Medical Research and the Canadian Diabetes Association. C.T. is a Clinical Investigator of the Alberta Heritage Foundation for Medical Research and D.W.Z. is a Scientist of the Alberta Heritage Foundation for Medical Research.

### References

Abbott MA, Wells DG, Fallon JR. The insulin receptor tyrosine kinase substrate p58/53 and the insulin receptor are components of CNS synapses. J Neurosci 1999; 19: 7300–7308.

Adamo M, Raizada MK, LeRoith D. Insulin and insulin-like growth factor receptors in the nervous system. Mol Neurobiol 1989; 3: 71–100.

Akisaki T, Sakurai T, Takata T, Umegaki H, Araki A, Mizuno S, et al. Cognitive dysfunction associates with white matter hyperintensities and subcortical atrophy on magnetic resonance imaging of the elderly diabetes mellitus Japanese elderly diabetes intervention trial (J-EDIT). Diabetes Metab Res Rev 2006; 22: 376–84.

Awad N, Gagnon M, Messier C. The relationship between impaired glucose tolerance, type 2 diabetes, and cognitive function. J Clin Exp Neuropsychol 2004; 26: 1044–80.

Baskin DG, Figlewicz DP, Woods SC, Porte D Jr, Dorsa DM. Insulin in the brain. Annu Rev Physiol 1987; 49: 335–47.

Benedict C, Hallschmid M, Hatke A, Schultes B, Fehm HL, Born J, et al. Intranasal insulin improves memory in humans. Psychoneuroendocrinology 2004; 29: 1326–34.

Benedict C, Hallschmid M, Schultes B, Born J, Kern W. Intranasal insulin to improve memory function in humans. Neuroendocrinology 2007; 86: 136–42.

Biessels GJ, Deary IJ, Ryan CM. Cognition and diabetes: a lifespan perspective. Lancet Neurol 2008; 7: 184–90.

Biessels GJ, Kamal A, Ramakers GM, Urban IJ, Spruijt BM, Erkelens DW, et al. Place learning and hippocampal synaptic plasticity in streptozotocin-induced diabetic rats. Diabetes 1996; 45: 1259–66.

Biessels GJ, Kamal A, Urban IJ, Spruijt BM, Erkelens DW, Gispen WH. Water maze learning and hippocampal synaptic plasticity in streptozotocin-diabetic rats: effects of insulin treatment. Brain Res 1998; 800: 125–35.

Bijur GN, De SP, Jope RS. Glycogen synthase kinase-3beta facilitates staurosporine- and heat shock-induced apoptosis. Protection by lithium. J Biol Chem 2000; 275: 7583–90.

Born J, Lange T, Kern W, McGregor GP, Bickel U, Fehm HL. Sniffing neuropeptides: a transnasal approach to the human brain. Nat Neurosci 2002; 5: 514–6.

Bruss MD, Arias EB, Lienhard GE, Cartee GD. Increased phosphorylation of Akt substrate of 160 kDa (AS160) in rat skeletal muscle in response to insulin or contractile activity. Diabetes 2005; 54: 41–50.

Burdo JR, Chen Q, Calcutt NA, Schubert D. The pathological interaction between diabetes and presymptomatic Alzheimer's disease. Neurobiol Aging 2008.

Chen XQ, Fawcett JR, Rahman YE, Ala TA, Frey II WH. Delivery of nerve growth factor to the brain via the olfactory pathway. J Alzheimers Dis 1998; 1: 35–44.

Cohen RA. Dysfunction of vascular endothelium in diabetes mellitus. Circulation 1993; 87: V67–76.

Cohen P, Frame S. The renaissance of GSK3. Nat Rev Mol Cell Biol 2001; 2: 769–76.

Craft S, Peskind E, Schwartz MW, Schellenberg GD, Raskind M, Porte D, Jr. Cerebrospinal fluid and plasma insulin levels in Alzheimer's disease: relationship to severity of dementia and apolipoprotein E genotype. Neurology 1998; 50: 164–8.

Craft S, Watson GS. Insulin and neurodegenerative disease: shared and specific mechanisms. Lancet Neurol 2004; 3: 169–78.

Crawley JN: Behavioral paradigms. The Morris water task. In: Crawley JN, editor. What's wrong with my mouse? Behavioral phenotyping of transgenic and knockout mice. New York: Wiley-Liss; 2000. p. 87–95.

Cui QL, Almazan G. IGF-I-induced oligodendrocyte progenitor proliferation requires PI3K/Akt, MEK/ERK, and Src-like tyrosine kinases. J Neurochem 2007; 100: 1480–93.

de Groot JC, de Leeuw FE, Oudkerk M, van GJ, Hofman A, Jolles J, Breteler MM. Cerebral white matter lesions and cognitive function: the Rotterdam Scan Study. Ann Neurol 2000; 47: 145–51.

Dhanda DS, Frey WH, Leopold D, Kompella UB. Nose to brain delivery: approaches for drug deposition in the human olfactory epithelium. Drug Deliv Technol 2005; 5: 64–72.

Dudek H, Datta SR, Franke TF, Birnbaum MJ, Yao R, Cooper GM, et al. Regulation of neuronal survival by the serine-threonine protein kinase Akt. Science 1997; 275: 661–5.

Fernyhough P, Huang TJ, Verkhratsky A. Mechanism of mitochondrial dysfunction in diabetic sensory neuropathy. J Peripher Nerv Syst 2003; 8: 227–35.

File SE, Wardill AG. The reliability of the hole-board apparatus. Psychopharmacologia 1975; 44: 47–51.

Fox MA, Chen RS, Holmes CS. Gender differences in memory and learning in children with insulin-dependent diabetes mellitus (IDDM) over a 4-year follow-up interval. J Pediatr Psychol 2003; 28: 569–78.

Frederick TJ, Min J, Altieri SC, Mitchell NE, Wood TL. Synergistic induction of cyclin D1 in oligodendrocyte progenitor cells by IGF-I and FGF-2 requires differential stimulation of multiple signaling pathways. Glia 2007; 55: 1011–22.

Freude S, Plum L, Schnitker J, Leeser U, Udelhoven M, Krone W, et al. Peripheral hyperinsulinemia promotes tau phosphorylation in vivo. Diabetes 2005; 54: 3343–8.

Grimes CA, Jope RS. CREB DNA binding activity is inhibited by glycogen synthase kinase-3 beta and facilitated by lithium. J Neurochem 2001; 78: 1219–32.

Gundersen HJ, Bendtsen TF, Korbo L, Marcussen N, Moller A, Nielsen K, et al. Some new, simple and efficient stereological methods and their use in pathological research and diagnosis. APMIS 1988; 96: 379–94.

Haan MN. Therapy Insight: type 2 diabetes mellitus and the risk of late-onset Alzheimer's disease. Nat Clin Pract Neurol 2006; 2: 159–66.

Hallschmid M, Benedict C, Schultes B, Born J, Kern W. Obese men respond to cognitive but not to catabolic brain insulin signaling. Int J Obes (Lond) 2008; 32: 275–82.

Hattori Y, Hattori S, Sato N, Kasai K. High-glucose-induced nuclear factor kappaB activation in vascular smooth muscle cells. Cardiovasc Res 2000; 46: 188–97.

Havrankova J, Schmechel D, Roth J, Brownstein M. Identification of insulin in rat brain. Proc Natl Acad Sci USA 1978a; 75: 5737–41.

Havrankova J, Roth J, Brownstein M. Insulin receptors are widely distributed in the central nervous system of the rat. Nature 1978b; 272: 827–9.

Heidenreich KA, Zahniser NR, Berhanu P, Brandenburg D, Olefsky JM. Structural differences between insulin receptors in the brain and peripheral target tissues. J Biol Chem 1983; 258: 8527–30.

Hetman M, Cavanaugh JE, Kimelman D, Xia Z. Role of glycogen synthase kinase-3beta in neuronal apoptosis induced by trophic withdrawal. J Neurosci 2000; 20: 2567–74.

Ho L, Qin W, Pompl PN, Xiang Z, Wang J, Zhao Z, et al. Diet-induced insulin resistance promotes amyloidosis in a transgenic mouse model of Alzheimer's disease. FASEB J 2004; 18: 902–4.

Hoyer S. Glucose metabolism and insulin receptor signal transduction in Alzheimer disease. Eur J Pharmacol 2004; 490: 115–25.

Huang C, Thirone AC, Huang X, Klip A. Differential contribution of insulin receptor substrates 1 versus 2 to insulin signaling and glucose uptake in l6 myotubes. J Biol Chem 2005a; 280: 19426–35.

Huang TJ, Verkhratsky A, Fernyhough P. Insulin enhances mitochondrial inner membrane potential and increases ATP levels through phosphoinositide 3-kinase in adult sensory neurons. Mol Cell Neurosci 2005b; 28: 42–54.

Ikram MA, Vrooman HA, Vernooij MW, van der LF, Hofman A, van der LA, et al. Brain tissue volumes in the general elderly population. The Rotterdam Scan Study. Neurobiol Aging 2008; 29: 882–90.

Jacobson AM, Musen G, Ryan CM, Silvers N, Cleary P, Waberski B, et al. Long-term effect of diabetes and its treatment on cognitive function. N Engl J Med 2007; 356: 1842–52.

Jones DM, Tucker BA, Rahimtula M, Mearow KM. The synergistic effects of NGF and IGF-1 on neurite growth in adult sensory neurons: convergence on the PI 3-kinase signaling pathway. J Neurochem 2003; 86: 1116–28.

Kaiyala KJ, Prigeon RL, Kahn SE, Woods SC, Schwartz MW. Obesity induced by a high-fat diet is associated with reduced brain insulin transport in dogs. Diabetes 2000; 49: 1525–33.

Kamal A, Biessels GJ, Duis SE, Gispen WH. Learning and hippocampal synaptic plasticity in streptozotocin-diabetic rats: interaction of diabetes and ageing. Diabetologia 2000; 43: 500–6.

Kamal A, Biessels GJ, Gispen WH, Ramakers GM. Synaptic transmission changes in the pyramidal cells of the hippocampus in streptozotocin-induced diabetes mellitus in rats. Brain Res 2006; 1073–1074: 276–80.

Khafagy E, Morishita M, Onuki Y, Takayama K. Current challenges in non-invasive insulin delivery systems: a comparative review. Adv Drug Deliv Rev 2007; 59: 1521–46.

Kloppenborg RP, van den Berg E, Kappelle LJ, Biessels GJ. Diabetes and other vascular risk factors for dementia: which factor matters most? A systematic review. Eur J Pharmacol 2008; 585: 97–108.

Knopman D, Boland LL, Mosley T, Howard G, Liao D, Szklo M, et al. Cardiovascular risk factors and cognitive decline in middle-aged adults. Neurology 2001; 56: 42–8.

Kramer L, Fasching P, Madl C, Schneider B, Damjancic P, Waldhausl W, et al. Previous episodes of hypoglycemic coma are not associated with permanent cognitive brain dysfunction in IDDM patients on intensive insulin treatment. Diabetes 1998; 47: 1909–14.

Last D, Alsop DC, Abduljalil AM, Marquis RP, de BC, Hu K, et al. Global and regional effects of type 2 diabetes on brain tissue volumes and cerebral vasoreactivity. Diabetes Care 2007; 30: 1193–9.

Leinninger GM, Backus C, Uhler MD, Lentz SI, Feldman EL. Phosphatidylinositol 3-kinase and Akt effectors mediate insulin-like growth factor-I neuroprotection in dorsal root ganglia neurons. FASEB J 2004; 18: 1544–6.

Leroy K, Brion JP. Developmental expression and localization of glycogen synthase kinase-3beta in rat brain. J Chem Neuroanat 1999; 16: 279–3.

Li ZG, Zhang W, Sima AA. The role of impaired insulin/IGF action in primary diabetic encephalopathy. Brain Res 2005; 1037: 12–24.

Li ZG, Zhang W, Sima AA. Alzheimer-like changes in rat models of spontaneous diabetes. Diabetes 2007; 56: 1817–24.

Liu XF, Fawcett JR, Hanson LR, Frey WH. The window of opportunity for treatment of focal cerebral ischemic damage with noninvasive intranasal insulin-like growth factor-I in rats. J Stroke Cerebrovasc Dis 2004; 13: 16–23.

Lonze BE, Riccio A, Cohen S, Ginty DD. Apoptosis, axonal growth defects, and degeneration of peripheral neurons in mice lacking CREB. Neuron 2002; 34: 371–85.

Lupien SB, Bluhm EJ, Ishii DN. Effect of IGF-I on DNA, RNA, and protein loss associated with brain atrophy and impaired learning in diabetic rats. Neurobiol Dis 2006; 21: 487–95.

Mahadev K, Wu X, Motoshima H, Goldstein BJ. Integration of multiple downstream signals determines the net effect of insulin on MAP kinase vs. PI 3′-kinase activation: potential role of insulin-stimulated H(2)O(2). Cell Signal 2004; 16: 323–31.

Manschot SM, Brands AM, van der GJ, Kessels RP, Algra A, Kappelle LJ, et al. Brain magnetic resonance imaging correlates of impaired cognition in patients with type 2 diabetes. Diabetes 2006; 55: 1106–13.

Marshall CJ. Specificity of receptor tyrosine kinase signaling: transient versus sustained extracellular signal-regulated kinase activation. Cell 1995; 80: 179–85.

Matsumoto H, Rhoads DE. Specific binding of insulin to membranes from dendrodendritic synaptosomes of rat olfactory bulb. J Neurochem 1990; 54: 347–50.

McCarthy AM, Lindgren S, Mengeling MA, Tsalikian E, Engvall JC. Effects of diabetes on learning in children. Pediatrics 2002; 109: E9.

Miles WR, Root HF. Psychologic tests applied to diabetic patients. Arch Intern Med 1922; 30: 767–77.

Mooradian AD. Central nervous system complications of diabetes mellitus–a perspective from the blood-brain barrier. Brain Res Brain Res Rev 1997; 23: 210–8.

Morris R. Developments of a water-maze procedure for studying spatial learning in the rat. J Neurosci Methods 1984; 11: 47–60.

Munoz DG, Hastak SM, Harper B, Lee D, Hachinski VC. Pathologic correlates of increased signals of the centrum ovale on magnetic resonance imaging. Arch Neurol 1993; 50: 492–7.

Musen G, Lyoo IK, Sparks CR, Weinger K, Hwang J, Ryan CM, et al. Effects of type 1 diabetes on gray matter density as measured by voxel-based morphometry. Diabetes 2006; 55: 326–33.

Murray AD, Staff RT, Shenkin SD, Deary IJ, Starr JM, Whalley LJ. Brain white matter hyperintensities: relative importance of vascular risk factors in nondemented elderly people. Radiology 2005; 237: 251–7.

Northam EA, Anderson PJ, Jacobs R, Hughes M, Warne GL, Werther GA. Neuropsychological profiles of children with type 1 diabetes 6 years after disease onset. Diabetes Care 2001; 24: 1541–6.

Ogata T, Iijima S, Hoshikawa S, Miura T, Yamamoto S, Oda H, et al. Opposing extracellular signal-regulated kinase and Akt pathways control Schwann cell myelination. J Neurosci 2004; 24: 6724–32.

Owens DR, Zinman B, Bolli G. Alternative routes of insulin delivery. Diabet Med 2003; 20: 886–98.

Pantoni L, Garcia JH. Pathogenesis of leukoaraiosis: a review. Stroke 1997; 28: 652–9.

Pantoni L, Poggesi A, Inzitari D. The relation between white-matter lesions and cognition. Curr Opin Neurol 2007; 20: 390–7.

Pap M, Cooper GM. Role of glycogen synthase kinase-3 in the phosphatidylinositol 3-Kinase/Akt cell survival pathway. J Biol Chem 1998; 273: 19929–32.

Patti ME, Sun XJ, Bruening JC, Araki E, Lipes MA, White MF, et al. 4PS/insulin receptor substrate (IRS)-2 is the alternative substrate of the insulin receptor in IRS-1-deficient mice. J Biol Chem 1995; 270: 24670–3.

Reaven GM, Thompson LW, Nahum D, Haskins E. Relationship between hyperglycemia and cognitive function in older NIDDM patients. Diabetes Care 1990; 13: 16–21.

Reger MA, Watson GS, Frey WH, Baker LD, Cholerton B, Keeling ML, et al. Effects of intranasal insulin on cognition in memory-impaired older adults: modulation by APOE genotype. Neurobiol Aging 2006; 27: 451–8.

Reger MA, Watson GS, Green PS, Wilkinson CW, Baker LD, Cholerton B, et al. Intranasal insulin improves cognition and modulates beta-amyloid in early AD. Neurology 2008; 70: 440–8.

Ross TM, Martinez PM, Renner JC, Thorne RG, Hanson LR, Frey WH. Intranasal administration of interferon beta bypasses the blood-brain barrier to target the central nervous system and cervical lymph nodes: a non-invasive treatment strategy for multiple sclerosis. J Neuroimmunol 2004; 151: 66–77.

Rothblat LA, Kromer LF. Object recognition memory in the rat: the role of the hippocampus. Behav Brain Res 1991; 42: 25–32.

Ryan CM. Neurobehavioral complications of type I diabetes. Examination of possible risk factors. Diabetes Care 1988; 11: 86–93.

Ryan CM, Williams TM. Effects of insulin-dependent diabetes on learning and memory efficiency in adults. J Clin Exp Neuropsychol 1993; 15: 685–700.

Ryan CM, Williams TM, Finegold DN, Orchard TJ. Cognitive dysfunction in adults with type 1 (insulin-dependent) diabetes mellitus of long duration: effects of recurrent hypoglycaemia and other chronic complications. Diabetologia 1993; 36: 329–34.

Ryan CM, Geckle M. Why is learning and memory dysfunction in Type 2 diabetes limited to older adults? Diabetes Metab Res Rev 2000; 16: 308–15.

Salkovic-Petrisic M, Tribl F, Schmidt M, Hoyer S, Riederer P. Alzheimer-like changes in protein kinase B and glycogen synthase kinase-3 in rat frontal cortex and hippocampus after damage to the insulin signalling pathway. J Neurochem 2006; 96: 1005–15.

Schoenle EJ, Schoenle D, Molinari L, Largo RH. Impaired intellectual development in children with Type I diabetes: association with HbA(1c), age at diagnosis and sex. Diabetologia 2002; 45: 108–14.

Schmidt R, Launer LJ, Nilsson LG, Pajak A, Sans S, Berger K, et al. Magnetic resonance imaging of the brain in diabetes: the Cardiovascular Determinants of Dementia (CASCADE) Study. Diabetes 2004; 53: 687–92.

Schwabe K, Klein S, Koch M. Behavioural effects of neonatal lesions of the medial prefrontal cortex and subchronic pubertal treatment with phencyclidine of adult rats. Behav Brain Res 2006; 168: 150–60.

Schwartz AV, Vittinghoff E, Sellmeyer DE, Feingold KR, de RN, Strotmeyer ES, et al. Diabetes-related complications, glycemic control, and falls in older adults. Diabetes Care 2008; 31: 391–6.

Stewart R, Liolitsa D. Type 2 diabetes mellitus, cognitive impairment and dementia. Diabet Med 1999; 16: 93–112.

Strachan MW, Deary IJ, Ewing FM, Frier BM. Is type II diabetes associated with an increased risk of cognitive dysfunction? A critical review of published studies. Diabetes Care 1997; 20: 438–45.

Stranahan AM, Arumugam TV, Cutler RG, Lee K, Egan JM, Mattson MP. Diabetes impairs hippocampal function through glucocorticoid-mediated effects on new and mature neurons. Nat Neurosci 2008; 11: 309–17.

Thorne RG, Pronk GJ, Padmanabhan V, Frey WH. Delivery of insulin-like growth factor-I to the rat brain and spinal cord along olfactory and trigeminal pathways following intranasal administration. Neuroscience 2004; 127: 481–96.

Tomlinson DR, Gardiner NJ. Glucose neurotoxicity. Nat Rev Neurosci 2008; 9: 36–45.

Benedict C, Kern W, Schultes B, Born J, Hallschmid M. Differential sensitivity of men and women to anorexigenic and memory improving effects of intranasal insulin. J Clin Endocrinol Metab 2008.

Toth C, Schmidt AM, Tuor UI, Francis G, Foniok T, Brussee V, et al. Diabetes, leukoencephalopathy and RAGE. Neurobiol Dis 2006; 23: 445–61.

Trejo JL, Llorens-Martín MV, Torres-Alemán I. The effects of exercise on spatial learning and anxiety-like behavior are mediated by an IGF-I-dependent mechanism related to hippocampal neurogenesis. Mol Cell Neurosci. 2008; 37: 402–11.

Tullberg M, Fletcher E, DeCarli C, Mungas D, Reed BR, Harvey DJ, et al. White matter lesions impair frontal lobe function regardless of their location. Neurology 2004; 63: 246–53.

Unger J, McNeill TH, Moxley RT, III, White M, Moss A, Livingston JN. Distribution of insulin receptor-like immunoreactivity in the rat forebrain. Neuroscience 1989; 31: 143–57.

Unger JW, Livingston JN, Moss AM. Insulin receptors in the central nervous system: localization, signalling mechanisms and functional aspects. Prog Neurobiol 1991; 36: 343–62.

van Harten B, de Leeuw FE, Weinstein HC, Scheltens P, Biessels GJ. Brain imaging in patients with diabetes: a systematic review. Diabetes Care 2006; 29: 2539–48.

van Harten B, Oosterman JM, Potter van Loon BJ, Scheltens P, Weinstein HC. Brain lesions on MRI in elderly patients with type 2 diabetes mellitus. Eur Neurol 2007; 57: 70–4.

Verdelho A, Madureira S, Ferro JM, Basile AM, Chabriat H, Erkinjuntti T, et al. Differential impact of cerebral white matter changes, diabetes, hypertension and stroke on cognitive performance among non-disabled elderly. The LADIS study. J Neurol Neurosurg Psychiatry 2007; 78: 1325–30.

Viard P, Butcher AJ, Halet G, Davies A, Nürnberg B, Heblich F, Dolphin AC. PI3K promotes voltage-dependent calcium channel trafficking to the plasma membrane. Nat Neurosci 2004; 7: 939–46.

Vig PJ, Subramony SH, D'Souza DR, Wei J, Lopez ME. Intranasal administration of IGF-I improves behavior and Purkinje cell pathology in SCA1 mice. Brain Res Bull 2006; 69: 573–9.

Walton M, Woodgate AM, Muravlev A, Xu R, During MJ, Dragunow M. CREB phosphorylation promotes nerve cell survival. J Neurochem 1999; 73: 1836–42.

Wan Q, Xiong ZG, Man HY, Ackerley CA, Braunton J, Lu WY, et al. Recruitment of functional GABA(A) receptors to postsynaptic domains by insulin. Nature 1997; 388: 686–90.

Weinger K, Jacobson AM, Musen G, Lyoo IK, Ryan CM, Jimerson DC, et al. The effects of type 1 diabetes on cerebral white matter. Diabetologia 2008; 51: 417–25.

Wessels AM, Rombouts SA, Remijnse PL, Boom Y, Scheltens P, Barkhof F, et al. Cognitive performance in type 1 diabetes patients is associated with cerebral white matter volume. Diabetologia 2007; 50: 1763–9.

White MF, Yenush L. The IRS-signaling system: a network of docking proteins that mediate insulin and cytokine action. Curr Top Microbiol Immunol 1998; 228: 179–208.

Whitman GT, Tang Y, Lin A, Baloh RW. A prospective study of cerebral white matter abnormalities in older people with gait dysfunction. Neurology 2001; 57: 990–4.

Wickelgren I. Tracking insulin to the mind. Science 1998; 280: 517–9.

Woods SC, Seeley RJ, Baskin DG, Schwartz MW. Insulin and the blood-brain barrier. Curr Pharm Des 2003; 9: 795–800.

Yao R, Cooper GM. Requirement for phosphatidylinositol-3 kinase in the prevention of apoptosis by nerve growth factor. Science 1995; 267: 2003–6.

Yoshiyama Y, Higuchi M, Zhang B, Huang SM, Iwata N, Saido TC, et al. Synapse loss and microglial activation precede tangles in a P301S tauopathy mouse model. Neuron 2007; 53: 337–51.

Yu XR, Jia GR, Gao GD, Wang SH, Han Y, Cao W. Neuroprotection of insulin against oxidative stress-induced apoptosis in cultured retinal neurons: involvement of phosphoinositide 3-kinase/Akt signal pathway. Acta Biochim Biophys Sin (Shanghai) 2006; 38: 241–8.

Zhao W, Chen H, Xu H, Moore E, Meiri N, Quon MJ, et al. Brain insulin receptors and spatial memory. Correlated changes in gene expression, tyrosine phosphorylation, and signaling molecules in the hippocampus of water maze trained rats. J Biol Chem 1999; 274: 34893–902.

Zhao WQ, Chen H, Quon MJ, Alkon DL. Insulin and the insulin receptor in experimental models of learning and memory. Eur J Pharmacol 2004a; 490: 71–81.

Zhao L, Teter B, Morihara T, Lim GP, Ambegaokar SS, Ubeda OJ, et al. Insulin-degrading enzyme as a downstream target of insulin receptor signaling cascade: implications for Alzheimer's disease intervention. J Neurosci 2004b; 24: 11120–6.

Zhao WQ, De Felice FG, Fernandez S, Chen H, Lambert MP, Quon MJ, et al. Amyloid beta oligomers induce impairment of neuronal insulin receptors. FASEB J 2008; 22: 246–60.

Zheng WH, Kar S, Quirion R. Insulin-like growth factor-1-induced phosphorylation of transcription factor FKHRL1 is mediated by phosphatidylinositol 3-kinase/Akt kinase and role of this pathway in insulin-like growth factor-1-induced survival of cultured hippocampal neurons. Mol Pharmacol 2002; 62: 225–33.



## Appendix I

The following brain regions were chosen as areas for close inspection within this study for MRI and myelin quantification portions of the experiment:

Caudate putamen
Primary motor/sensory cortex
Internal capsule
Cerebral peduncle
CA1 region of hippocampus
CA2/3 region of hippocampus
Ventroposterior region of thalamus
Corpus callosum
Amygdala
Substantia nigra pars reticulata
Subiculum
Lentiform nuclear region
Primary visual cortex
Cerebellum